Shear deformable plate by SGBEM: indirect “progenitor matrix” approach.

S.S. Terravecchia*

*Dipartimento di Ingegneria, Area Strutture, Università di Palermo, Viale delle Scienze, 90128, Sicilia, Italia.

Email address: silviosalvatore.terravecchia@unipa.it

Abstract

The Mindlin-Reissner’s formulation of shear deformable plate is addressed through the Symmetric Galerkin Boundary Element Method (SGBEM). The thick plate’s elastic problem is resolved and fundamental solutions matrix is obtained. The application of Betti's theorem in the unlimited domain allows obtaining the Somigliana’s Identities (S.I.s). The solving system is obtained by an indirect approach, i.e., through the “progenitor matrix”. The “progenitor matrix” allows simulating all possible plate’s load conditions and is the starting point for an automatic calculation code. The coefficients are calculated through the theory of distributions, using double integrals without resorting to regularization techniques but by exploiting the expansion in power series of the Bessel functions present in the fundamental solutions.

Particular attention is paid to the presence of domain loads, whose domain integral is transformed into a boundary one using the Radial Integral Method technique (RIM).

These strategies lead to a robust procedure that allows obtaining good results even in the presence of boundary sparse discretization. This is demonstrated by the results of the examples carried out which, compared with the analytical solutions present in the literature, show very a good convergence.

Keywords: SGBEM, shear deformable plate, progenitor matrix, RIM technique.

1. Introduction

The present work is based on the SGBEM that has shown its big potentiality in the last decades. SGBEM, introduced by the pioneering work of Sirtori [1], is formulated in Polizzotto [2] through the Hu-Washizu theorem. An extensive dissertation on the topics treated with SGBEM can be found in the paper of Bonnet et. al. [3].

The SGBEM approach shows advantages that can be summarized as follows: it provides an energetic meaning to the formulation of boundary integral equations; the symmetry and definiteness of the operators allows demonstrating the existence and uniqueness of the solution; the load vector reflects the real distribution of external actions; moreover, as in the classic BEM, the use of fundamental solutions guarantees compatibility and equilibrium at any point on the boundary and in the domain.

The disadvantages of the method are related to the computational aspects due to the presence of double integrals with divergent kernels; an exhaustive discussion of these topics can be found in Terravecchia [4]. Other are: presence of domains with different physical and mechanical characteristics and computational difficulties in handling domain loads; an exhaustive bibliography of these problems can be found in Panzeca [5, 6] where solutions are provided.

In the area of shear deformable plates, Reissner [7-8] and Mindlin [9] have developed a general theory which can be used for both thin and thick plates; in this way the problems associated with Kirchhoff's theory, leading in some cases to inadequate results, can be avoided.

Shear deformable plates have received considerable attention in the field of collocation BEM. The first applications to the Reissner’s model are due to Vander Weeën [10] who derives the fundamental solutions through the Hörmander’s method [11] and the loads distributed on the plate’s surface are integrated on the boundary both through the application of the divergence theorem and the use of particular solutions. El Zafrany [12] obtains the fundamental solutions using the integral Hankel transform and in [13] provides fundamental solutions valid for thick and thin plates; the terms representing the shear effects are provided separately and their exclusion allows analyzing the thin plates. Westphal et al [14] study the fundamental solutions of the Mindlin-Reissner’s model and the relationships with Kirchhoff's classical model; they show that Mindlin Reissner's general model solution includes that of Kirchhoff's classical model. Always for the Reissner’s model, Long et al [15] propose a formulation involving three integral equations, which can be applied not only to moderately thick plates, but also to plates usually analysed by classical Kirchhoff’s theory. Rashed [16] presents the hypersingular boundary element formulation and use rigid body considerations together with the Taylor expansion (Aliabadi [17]) to compute the hypersingular kernels; the results obtained through the S.I.s of the displacements and tractions are compared with the analytical solution. The most recent developments in plate bending, together with an adequate bibliography may be found in Aliabadi [18, 19].

In the area of the SGBEM, the topic of the shear deformable plate receives little attention. Perez-Gavilan and Aliabadi [20] provide one of the main contributions. In [20] a different treatment of the S.I.s is carried out based on the singularities present in them. All S.I.s are subject to a regularization process which consists, depending on the singularity, in the subtraction of one or more terms of the Taylor series expansion around the source point and the added back-term are re-interpreted: in the displacement equations using the known kernel properties obtained using rigid body translation and rotation modes; in the moment equations using known kernel properties or as Cauchy principal value; in the shear equation

using new kernel identies obtained from a constant shear mode of deformation. Regularized forms of the S.I.s are obtained except for the shear's S.I, which shows a strong singularity on the corners. The same authors [21] develop a SGBEM formulation for shear deformable plate bending in dynamics using the static fundamental solutions.
In this paper, the solving system is obtained through an indirect approach called for "progenitor matrix". The latter is a generalized approach that considers the solid object of analysis imbedded in an unlimited domain that must remain unstressed and not deformed when the solution is obtained. The set of displacement and traction S.I.s is written for the entire solid without taking into account the effective boundary conditions; the generation of the "progenitor matrix" is controlled by exploiting rigid motion techniques (rotation and translation) [5]. The approach has advantage of making available, for given physical and mechanical plate's characteristics, a matrix of coefficients. The reordering and subsequent partitioning of this matrix, based on the kinematic and mechanical conditions of the boundary, allows determining the matrix of the solution system and the boundary load vectors for all possible conditions (traction and displacement imposed on the boundary).This approach, like the direct approach, within the SGBEM, presents computational difficulties due to the presence in the "progenitor matrix" of double integrals with divergent nuclei.
In this paper, the computation of the double integral having hypersingular kernels, does not apply any consolidated technique in the context of SGBEM. The approach, here proposed, is based in interpreting the integral nucleus as distribution [4, 22]. Differently from other methods, it involves that the calculus of the coefficient may be made by considering the effect point directly on the boundary. This way of interpreting the function of the hypersingular nucleus permits to compute the integral, independently of the asymptotic behaviour of the function. In order to apply the technique it is necessary to isolate, in the fundamental solutions, expressed through the Bessel's functions of the second kind and $n-th$ order, the hypersingular part. This goal is achieved through the expansion in power series of the Bessel functions [Appendix 1]; this makes it possible to distinguish a singular part and a regular part in the integrals kernel. The coefficient's hypersingular part, of small dimensions, is calculated analytically by applying the theory of distributions; the coefficient's regular part, whose size is related to the number of terms of the series expansion, is calculated through numerical integration techniques. The optimal terms number of the coefficient's regular part that are considered in the calculation is determined through rigid motion techniques, being known the internal field of displacements and tractions. This makes the procedure particularly robust and the solution's convergence depends both on the discretization of the boundary and on the type of shape functions.
The "progenitor matrix" approach can also be applied in the collocation BEM and give rise to two distinct methods. An outline of this approach is already present in Brebbia et al. [23]. The collocation BEM with respect to the SGBEM uses a reduced number of fundamental solutions. It consists in the writing of the S.I.s. of displacements (displacement method) or that of tractions (tractions method); the boundary quantities of the problem are modelling through appropriate shape functions and the S.I.s are not subject to the weighting process as in the SGBEM approach with the consequence that the "progenitor matrix" is not symmetric. Even in this case, appropriate partitions and reorders allow obtaining the solving system matrix and the load vectors. In calculating the influence coefficients, the following are taken into account: the singularities present in the fundamental solutions used and the techniques necessary for their removal; the fact that the free term matrices are different from those used in the SGBEM.
In this paper, particular attention is paid to the vertical domain load vector that is generated separately through a RIM technique, Gao [24], Panzeca [6], valid for any variation law of domain load. The domain integrals are transformed into ones to be performed on the boundary, through a unified procedure, without introducing particular solutions or divergence theorem application. Fundamental modified solutions are obtained which are suitable to be integrated on the boundary and provide regular displacement and traction fields on the domain and on the boundary. The main feature of modified solutions, very important for the computational aspects, is that they are null when source point and effect point coincide. The RIM technique is applied directly to the domain integrals present in the displacements S.I. characterized by strong singularity.
In case of hypersingularity, as happens in the tractions S.I., the fundamental solutions are treated through regularization techniques and RIM technique. These combined techniques make it is possible to obtain the tractions S.I. with a regularized domain integral to which is added a boundary integral and a vector called Bui Free Term. The RIM technique allows considering the domain loads in their effective distribution, without approximations as happens in Wen [25] through the Radial Basis Functions (RBF).
This work presents: a general approach called "progenitor matrix" and the computation of its hypersingular coefficients through the application of distribution theory and the expansion in power series of the Bessel functions; the calculation of domain vertical load vector through the RIM technique, the latter being a general technique applicable to any load distribution.
This study constitutes the starting point for the implementation of an automatic calculation code operating in the field of plate substructuring approach, as already done for flat two-dimensional structures subject to actions acting in its plane [26]. This will allow proceed with the plate-to-plate coupling avoiding the very difficult treatment of the fundamental 3D solutions in the context of the SGBEM.

2. Elastostatic problem solution: the matrix of fundamental solutions.

Let us consider the plate of Fig. 1 referred to the general Cartesian reference system $O \equiv (x, y, z)$; the medium surface coincides with the plane (x, y) and the mechanical quantities are evaluated on the element dS, whose position is identified by the normal vector $\mathbf{n}$ and the counter clockwise tangent vector $\mathbf{t}$; in this reference system one writes:

$$\mathbf{m}_n = \begin{bmatrix} M_{nx} \\ M_{ny} \end{bmatrix} = \begin{bmatrix} M_{xx} & M_{xy} \\ M_{yx} & M_{yy} \end{bmatrix} \cdot \begin{bmatrix} n_x \\ n_y \end{bmatrix}; \; \mathbf{t}_n = [T_n]; \; \mathbf{u}^T = \begin{bmatrix} \varphi_x & \varphi_y & u_z \end{bmatrix} \tag{1a, b, c}$$

The traction vectors $\mathbf{m}_n$ $\mathbf{t}_n$ are referred to the unit of length evaluated on dS and to the thickness h of the plate.

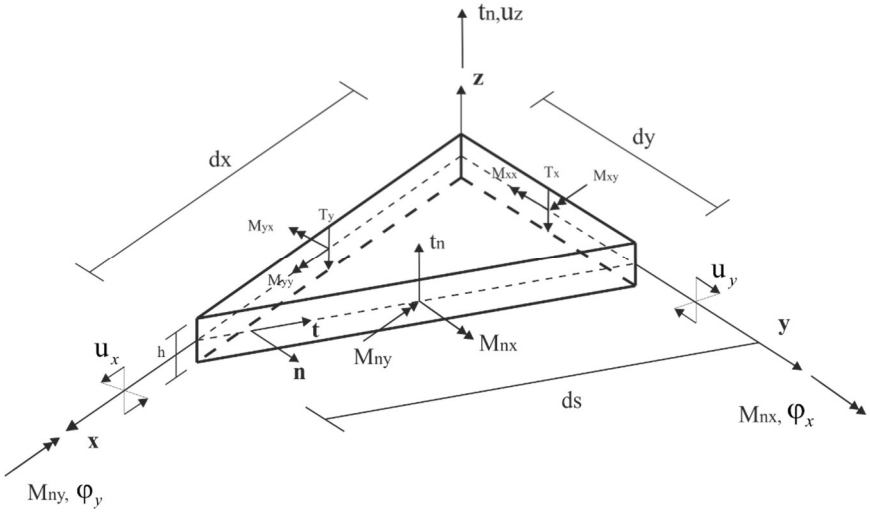

Fig. 1. General Cartesian reference system $O \equiv (x, y, z)$: vectors $\mathbf{m}_n$ $\mathbf{t}_n$ $\mathbf{u}$.

The moments and shears generalized vectors are

$$\mathbb{m} = \begin{bmatrix} M_{xx} \\ M_{yy} \\ M_{xy} \end{bmatrix} = \int_{-\frac{h}{2}}^{\frac{h}{2}} z\,\boldsymbol{\sigma}\, dz, \quad \mathbb{t} = \begin{bmatrix} T_x \\ T_y \end{bmatrix} = \int_{-\frac{h}{2}}^{\frac{h}{2}} \boldsymbol{\tau}\, dz \tag{2a, b}$$

in which the stress vectors $\boldsymbol{\sigma}^T = \begin{bmatrix} \sigma_{xx} & \sigma_{yy} & \tau_{xy} \end{bmatrix}$ and $\boldsymbol{\tau}^T = \begin{bmatrix} \tau_{xz} & \tau_{yz} \end{bmatrix}$ have respectively linear and parabolic distribution along plate's height.

If we define a traction vector $\mathbf{t}^T = \begin{bmatrix} \mathbf{m}_n^T & \mathbf{t}_n^T \end{bmatrix}$ and a generalized stress vector $\mathbf{s}^T = \begin{bmatrix} \mathbb{m}^T & \mathbb{t}^T \end{bmatrix}$ through the Cauchy's relation one writes

$$\mathbf{t} = \mathbf{N}_x \, \mathbf{s} \tag{3}$$

in which $\mathbf{N}_x$ is a matrix of director cosines.

The plate of domain Ω, boundary $\Gamma = \Gamma_1 + \Gamma_2$, made of homogeneous and isotropic material (Fig. 2) is subject to the following actions:

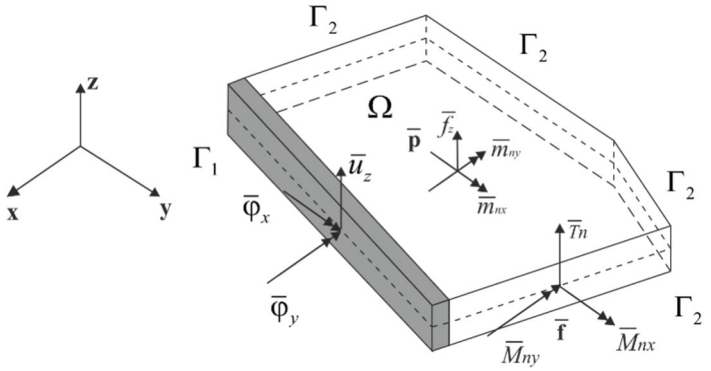

Fig. 2. Plate of domain Ω and boundary $\Gamma = \Gamma_1 + \Gamma_2$ subject to boundary and domain loading conditions.

- tractions $\bar{\mathbf{f}}^T = [\bar{M}_{nx} \quad \bar{M}_{ny} \quad \bar{T}_n]^T$ on the free boundary Γ_2;
- imposed displacements $\bar{\mathbf{u}}^T = [\bar{\varphi}_x \quad \bar{\varphi}_y \quad \bar{u}_z]^T$ on the constrained boundary Γ_1;
- surface tractions $\bar{\mathbf{p}}^T(x, y) = [\bar{m}_{nx}(x, y) \quad \bar{m}_{ny}(x, y) \quad \bar{f}_z(x, y)]^T$ on Ω.

The stress $\bar{\sigma}_z$, not considered in the Mindlin's model, in Reissner's model depends on the surface load $\bar{f}_z(x,y)$ according to the law

$$\bar{\sigma}_z(x,y,z) = \frac{\bar{f}_z(x,y)}{2} + \frac{\bar{f}_z(x,y)}{2}\left(\frac{3z}{h} - \frac{4z^3}{h^3}\right). \tag{4}$$

The solution of the Mindlin-Reissner's plate elastic problem is obtained through the system of equations:

$$\mathbf{q} = \mathbf{C}\,\mathbf{u} \tag{5}$$

$$\mathbf{s} = \mathbf{D}\,\mathbf{q} + H\,\mathbf{c}\,\bar{f}_z(x,y) \tag{6}$$

$$\mathbf{B}\,\mathbf{s} + \bar{\mathbf{p}} = \mathbf{0} \tag{7}$$

In the compatibility Eq. (5), $\mathbf{q}$ is the vector of generalized bending, torsion and shear strains, $\mathbf{C}$ is a matrix of differential operators and $\mathbf{u}$ is the displacement vector of the kinematic model highlighted in Fig. 1. In the constitutive Eq. (6), $\mathbf{s}$ is the generalized stress vector previously defined, $\mathbf{D}$ is the diagonal stiffness matrix of plate containing bending stiffness and the shear stiffness coefficients, $H = \nu/(1-\nu)\lambda^2$ the Reissner's model factor, $\lambda^2 = 10/h^2$ the shear factor and $\mathbf{c}$ an influence vector. In the equilibrium Eq. (7), $\mathbf{B}$ is a matrix of differential operators and $\bar{\mathbf{p}}$ the surface tractions vector previously defined.
The Eqs. (5-7), replaced progressively, allow determining the Navier's differential equations of the problem in the form

$$\mathbf{L}\,\mathbf{u} = -\mathbf{f} \tag{8}$$

where $\mathbf{L} = \mathbf{B}\,\mathbf{D}\,\mathbf{C}$ is a matrix of differential operators

$$\mathbf{L} = \begin{bmatrix} A(\nabla^2 - \frac{1+\nu}{2}\frac{\partial^2}{\partial y^2}) - \lambda_0 & A\frac{1+\nu}{2}\frac{\partial^2}{\partial x \partial y} & -\lambda_0\frac{\partial}{\partial x} \\ A\frac{1+\nu}{2}\frac{\partial^2}{\partial x \partial y} & A(\nabla^2 - \frac{1+\nu}{2}\frac{\partial^2}{\partial x^2}) - \lambda_0 & -\lambda_0\frac{\partial}{\partial y} \\ \lambda_0\frac{\partial}{\partial x} & \lambda_0\frac{\partial}{\partial y} & \lambda_0\nabla^2 \end{bmatrix} \tag{9}$$

and $\mathbf{f}$ the obtaing load term.

In the matrix $\mathbf{L}$, $A = E\,h^3/12(1-\nu^2)$ is the bending stiffness coefficient with E Young modulus, h height of the plate, ν Poisson's coefficient, $\lambda_0 = Gh/\chi$ is the shear stiffness of a rectangular section with G shear modulus and χ shear factor of rectangular section.

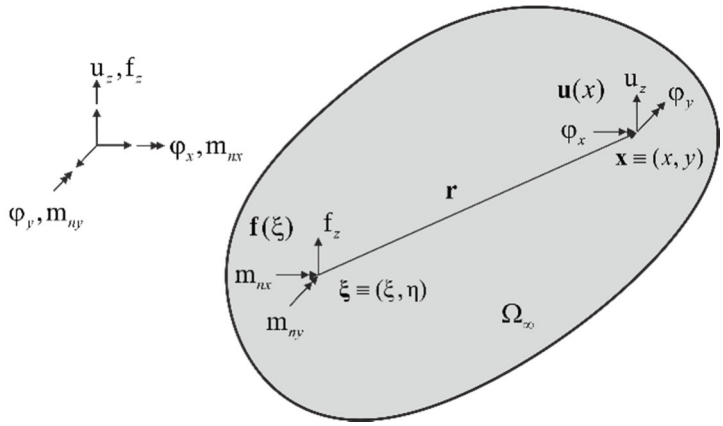

Fig. 3. Source point $\boldsymbol{\xi}$ with singular applied vector $\mathbf{f}(\xi)$, effect point with vector displacement $\mathbf{u}(\mathbf{x})$, vector distance $\mathbf{r}$.

If in Eq. (8) set $\mathbf{f} = \mathbf{I}\,\boldsymbol{\Delta}(\mathbf{x}-\boldsymbol{\xi})$ in which $\mathbf{I}$ is an identity matrix of order 3×3 and $\boldsymbol{\Delta}(\mathbf{x}-\boldsymbol{\xi})$ a Dirac Delta vector, it is possible to get, through the method of Hörmander [11] and introduced by Weeën [10], the matrix $\mathbf{G}_{uu}(\mathbf{x},\boldsymbol{\xi})$ of fundamental solutions valid in Ω_∞ Fig. 3. This matrix allows determining at the effect point $\mathbf{x} \equiv (x,y)$ the displacements

$\mathbf{u}(\mathbf{x})^T = [\varphi_x \quad \varphi_y \quad u_z]^T$ due to a singularity vector $\mathbf{f}(\boldsymbol{\xi})^T = [m_{nx} \quad m_{nx} \quad f_z]^T$ applied at the source point $\boldsymbol{\xi} \equiv (\xi, \eta)$ with $\mathbf{r} = \sqrt{\mathbf{x}^2 - \boldsymbol{\xi}^2}$ that is:

$$\mathbf{u}(\mathbf{x}) = \mathbf{G}_{uu}(\mathbf{x};\boldsymbol{\xi})\mathbf{f}(\boldsymbol{\xi}) \tag{10}$$

The matrix of fundamental solutions $\mathbf{G}_{uu}(\mathbf{x},\boldsymbol{\xi})$, allows finding [2] the complete matrix of fundamental solutions $\mathbf{G}(\mathbf{x};\boldsymbol{\xi})$ used in the context of the SGBEM approach (Table 1); the latter provide the plate response in Ω_∞ to the different applied actions.

Effects at **x** \ Causes at **x**	**f**	**-u**	**q**	**s**
u	$\mathbf{G}_{uu}(\mathbf{x};\boldsymbol{\xi})$	$\mathbf{G}_{ut}(\mathbf{x};\boldsymbol{\xi},\mathbf{n})$	$\mathbf{G}_{us}(\mathbf{x};\boldsymbol{\xi})$	$\mathbf{G}_{uq}(\mathbf{x};\boldsymbol{\xi})$
t	$\mathbf{G}_{tu}(\mathbf{x},\boldsymbol{\nu};\boldsymbol{\xi})$	$\mathbf{G}_{tt}(\mathbf{x},\boldsymbol{\nu};\boldsymbol{\xi},\mathbf{n})$	$\mathbf{G}_{ts}(\mathbf{x},\boldsymbol{\nu};\boldsymbol{\xi})$	$\mathbf{G}_{tq}(\mathbf{x},\boldsymbol{\nu};\boldsymbol{\xi})$
s	$\mathbf{G}_{su}(\mathbf{x};\boldsymbol{\xi})$	$\mathbf{G}_{st}(\mathbf{x};\boldsymbol{\xi},\mathbf{n})$	$\mathbf{G}_{ss}(\mathbf{x};\boldsymbol{\xi})$	$\mathbf{G}_{sq}(\mathbf{x};\boldsymbol{\xi})$
q	$\mathbf{G}_{qu}(\mathbf{x};\boldsymbol{\xi})$	$\mathbf{G}_{qt}(\mathbf{x};\boldsymbol{\xi},\mathbf{n})$	$\mathbf{G}_{qs}(\mathbf{x};\boldsymbol{\xi})$	$\mathbf{G}_{qq}(\mathbf{x};\boldsymbol{\xi})$

Table 1. Fundamental solutions for Mindlin-Reissner's plate.

The fundamental solutions matrix $\mathbf{G}_{hk}$ in Table 1 is characterized by two subscripts: the first indicates the effects in $\mathbf{x}$, i.e. displacement for $h = u$, traction for $h = t$, generalized stress for $h = s$, generalized strain for $h = q$; the second subscript indicates, through a work-coniugate rule, the cause applied at $\boldsymbol{\xi}$, i.e. a unit concentrated force $k = u$, a unit surface relative displacement for $k = t$, a unit imposed generalized strain for $k = s$, a unit imposed generalized stress for $k = q$.

The matrix of the fundamental solutions exhibits symmetries

$$\mathbf{G}_{hh}(\mathbf{x};\boldsymbol{\xi}) = \mathbf{G}_{hh}(\boldsymbol{\xi};\mathbf{x}) \quad h = u,t,s,q \tag{11}$$

$$\mathbf{G}_{hk}(\mathbf{x};\boldsymbol{\xi}) = \mathbf{G}_{kh}^T(\boldsymbol{\xi};\mathbf{x}) \;\; h \neq k, \quad h,k=u,t,s,q \tag{12}$$

which can be proved through energy theorems (Maxwell, Colonnetti, Volterra).

The fundamental solutions present in Table.1 show orders of singularity, up to r^{-2} in the column related to $-\mathbf{u}$ and in the row related to $\mathbf{t}$; these solutions all derive from $\mathbf{G}_{uu}(\mathbf{x};\boldsymbol{\xi})$. The fundamental solutions of Tab.1 are characterized by the presence of Bessel functions $K_n(z)$ of second kind and $n-th$ order, with $z = \lambda r$, which present singularities starting from the maximum order αz^{-n} and $\alpha = (n-1)!/2^{(1-n)}$ as evidenced by their expansion in power series (Magno [30]) given in Appendix 1.

Appendix 2 provides $\mathbf{G}_{uu}(\mathbf{x};\boldsymbol{\xi})$ fundamental solution in such a way that it is possible to identify his order of singularity: in fact, within parentheses to the present singularities of order αz^{-n} , the Bessel functions $K_n(z)$ having the same singularity are subtracted.

3. Somigliana's Identities and boundary integral equations.

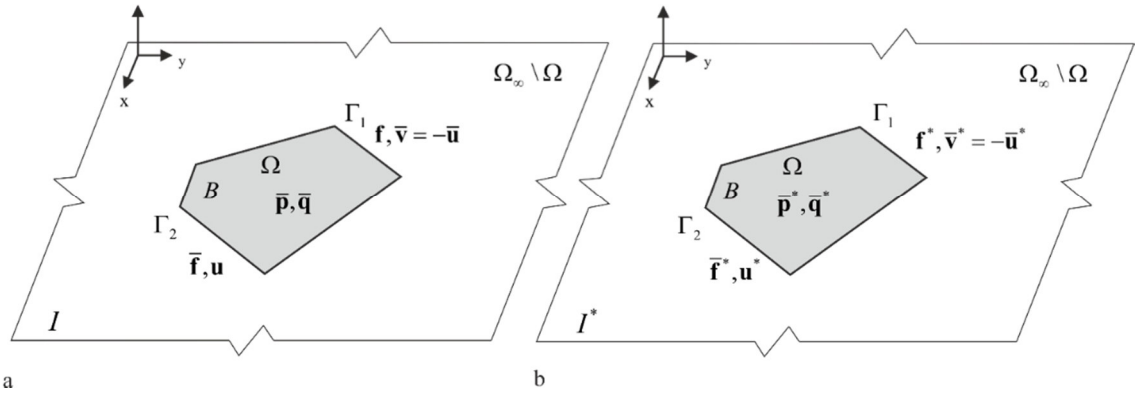

Fig. 4. Plate imbedded in the unlimited domain, a, b) system I and I^* with boundary and domain actions.

While the fundamental solutions provide the response in a point of the unlimited domain Ω_∞, the response to the distributed actions is provided by the S.I.s that are obtained by generalized Betti's theorem for elastic materials. Let us consider plate B imbedded in the unlimited domain Ω_∞ (Fig. 4) and two material systems: I and I^* systems.

The material system I is subject to:

- surface tractions $\overline{\mathbf{p}}$ in Ω;
- volumetric distortions $\overline{\mathbf{q}}$ in Ω;
- double-layered displacements $\overline{\mathbf{v}}(\mathbf{x}) = -\overline{\mathbf{u}}(\mathbf{x})$ in Γ_1;
- layered forces $\overline{\mathbf{f}}(\mathbf{x})$ in Γ_2.

The response to such actions are the vectors: $\mathbf{u}(\mathbf{x})$; $\mathbf{q}(\mathbf{x})$; $\mathbf{s}(\mathbf{x})$.

The material system $I*$ is subject to:

- surface tractions $\overline{\mathbf{p}}^*$ in Ω;
- volumetric distortions $\overline{\mathbf{q}}^*$ in Ω;
- double-layered displacements $\overline{\mathbf{v}}^*(\mathbf{x}) = -\overline{\mathbf{u}}^*(\mathbf{x})$ in Γ_1;
- layered forces $\overline{\mathbf{f}}^*(\mathbf{x})$ in Γ_2.

The response to such actions are the vectors: $\mathbf{u}^*(\mathbf{x})$; $\mathbf{q}^*(\mathbf{x})$; $\mathbf{s}^*(\mathbf{x})$.

The generalized Betti theorem valid for the unlimited domain Ω_∞ / Ω, with $\Gamma = \Gamma_1 \cup \Gamma_2$, is written:

$$\int_\Omega \left(\overline{\mathbf{p}}^*\right)^T \mathbf{u}\, d\Omega + \int_\Omega \left(\overline{\mathbf{q}}^*\right)^T \mathbf{s}\, d\Omega = \int_\Gamma \left(\mathbf{u}^*\right)^T \mathbf{f}\, d\Gamma + \int_\Gamma \left(\mathbf{f}^*\right)^T (-\mathbf{u})\, d\Gamma + \int_\Omega \left(\mathbf{u}^*\right)^T \overline{\mathbf{p}}\, d\Omega + \int_\Omega \left(\overline{\mathbf{s}}^*\right)^T \overline{\mathbf{q}}\, d\Omega \tag{13}$$

From Eq. (13) we obtain the S.I.s that provide the plate response subjected to actions distributed on the boundary $\Gamma = \Gamma_1 \cup \Gamma_2$ and on the domain Ω; keeping in mind the constitutive law Eq. (6) one can write:

- **S.I of displacements**
  If in Eq. (13) is set, $\overline{\mathbf{p}}^*(\mathbf{x}) = \mathbf{I}\,\Delta(\mathbf{x}-\boldsymbol{\xi})$; $\overline{\mathbf{q}}^* = \mathbf{0}$, the S.I of the displacements $\mathbf{u}(\mathbf{x})$ is obtained:

$$\begin{aligned}\mathbf{u}(\mathbf{x}) = &\int_\Gamma \mathbf{G}_{uu}(\mathbf{x};\boldsymbol{\xi})\mathbf{f}\, d\Gamma + \int_\Gamma \mathbf{G}_{ut}(\mathbf{x};\boldsymbol{\xi},\mathbf{n})(-\mathbf{u})\, d\Gamma + \int_\Omega \mathbf{G}_{us}(\mathbf{x};\boldsymbol{\xi})\overline{\mathbf{q}}\, d\Omega + \\ &+ \int_\Omega \mathbf{G}_{uu}(\mathbf{x};\boldsymbol{\xi})\overline{\mathbf{p}}\, d\Omega - H\int_\Omega \mathbf{G}_{uq}(\mathbf{x};\boldsymbol{\xi})\mathbf{c}\,\overline{f}_z(\xi,\eta)\, d\Omega\end{aligned} \tag{14}$$

- **S.I of generalized strains**
  If in Eq. (13) is set, $\overline{\mathbf{p}}^*(\mathbf{x}) = \mathbf{0}$; $\overline{\mathbf{q}}^* = \mathbf{D}^{-1}\overline{\mathbf{s}}^*$; $\overline{\mathbf{s}}^* = \Delta(\mathbf{x}-\boldsymbol{\xi})$, the S.I. of the generalized strain $\mathbf{q}(\mathbf{x})$ is obtained:

$$\begin{aligned}\mathbf{q}(\mathbf{x}) = &\int_\Gamma \mathbf{G}_{qu}(\mathbf{x};\boldsymbol{\xi})\mathbf{f}\, d\Gamma + \int_\Gamma \mathbf{G}_{qt}(\mathbf{x};\boldsymbol{\xi},\mathbf{n})(-\mathbf{u})\, d\Gamma + \int_\Omega \mathbf{G}_{qs}(\mathbf{x};\boldsymbol{\xi})\overline{\mathbf{q}}\, d\Omega + \\ &+ \int_\Omega \mathbf{G}_{qu}(\mathbf{x};\boldsymbol{\xi})\overline{\mathbf{p}}\, d\Omega - H\int_\Omega \mathbf{G}_{qq}(\mathbf{x};\boldsymbol{\xi})\mathbf{c}\,\overline{f}_z(\xi,\eta)\, d\Omega\end{aligned} \tag{15}$$

- **S.I of generalized stresses**
  If in Eq. (13) is set, $\overline{\mathbf{p}}^*(\mathbf{x}) = \mathbf{0}$; $\overline{\mathbf{q}}^*(\mathbf{x}) = \mathbf{I}\,\Delta(\mathbf{x}-\boldsymbol{\xi})$, the S.I. of the generalized stress $\mathbf{s}(\mathbf{x})$ is obtained:

$$\begin{aligned}\mathbf{s}(\mathbf{x}) = &\int_\Gamma \mathbf{G}_{su}(\mathbf{x};\boldsymbol{\xi})\mathbf{f}\, d\Gamma + \int_\Gamma \mathbf{G}_{st}(\mathbf{x};\boldsymbol{\xi},\mathbf{n})(-\mathbf{u})\, d\Gamma + \int_\Omega \mathbf{G}_{ss}(\mathbf{x};\boldsymbol{\xi})\overline{\mathbf{q}}\, d\Omega + \\ &+ \int_\Omega \mathbf{G}_{su}(\mathbf{x};\boldsymbol{\xi})\overline{\mathbf{p}}\, d\Omega - H\int_\Omega \mathbf{G}_{sq}(\mathbf{x};\boldsymbol{\xi})\mathbf{c}\,\overline{f}_z(\xi,\eta)\, d\Omega + \mathbf{c}\,\overline{f}_z(\xi,\eta)\end{aligned} \tag{16}$$

- **S.I of tractions**
  If in Eq. (13) is set, $\overline{\mathbf{p}}^*(\mathbf{x}) = \mathbf{0}$; $\overline{\mathbf{q}}^* = \mathbf{N}\,\Delta(\mathbf{x}-\boldsymbol{\xi})$, the S.I. of tractions $\mathbf{t}(\mathbf{x})$ is obtained:

$$\begin{aligned}\mathbf{t}(\mathbf{x},,\mathbf{v}) = &\int_\Gamma \mathbf{G}_{tu}(\mathbf{x},\mathbf{v};\boldsymbol{\xi})\mathbf{f}\, d\Gamma + \int_\Gamma \mathbf{G}_{tt}(\mathbf{x},\mathbf{v};\boldsymbol{\xi},\mathbf{n})(-\mathbf{u})\, d\Gamma + \int_\Omega \mathbf{G}_{ts}(\mathbf{x},\mathbf{v};\boldsymbol{\xi})\overline{\mathbf{q}}\, d\Omega + \\ &+ \int_\Omega \mathbf{G}_{tu}(\mathbf{x},\mathbf{v};\boldsymbol{\xi})\overline{\mathbf{p}}\, d\Omega - H\int_\Omega \mathbf{G}_{tq}(\mathbf{x},\mathbf{v};\boldsymbol{\xi})\mathbf{c}\,\overline{f}_z(\xi,\eta)\, d\Omega + \mathbf{N}_x\,\mathbf{c}\,\overline{f}_z(\xi,\eta)\end{aligned} \tag{17}$$

The S.I.s of the displacements (14) and tractions (17) used in the SGBEM approach, in the absence of inelastic actions $\overline{\mathbf{q}}$, are re-written considering the only component $\overline{f}_z(\xi,\eta)$ of the vector $\overline{\mathbf{p}}$.

$$\mathbf{u}(\mathbf{x}) = \int_{\Gamma} \mathbf{G}_{uu}(\mathbf{x};\xi)\mathbf{f}\,\mathrm{d}\Gamma + \underbrace{\int_{\Gamma} \mathbf{G}_{ut}(\mathbf{x};\xi,\mathbf{n})(-\mathbf{u})\,\mathrm{d}\Gamma}_{\text{discontinous on }\Gamma} + \int_{\Omega} \left(\mathbf{G}_{uu}^{\alpha,3}(\mathbf{x};\xi) - H\,\mathbf{G}_{uq}^{\alpha,\beta}(\mathbf{x};\xi)\right)\overline{f}_z(\xi,\eta)\,\mathrm{d}\Omega \tag{18}$$

$$\mathbf{t}(\mathbf{x},\mathbf{v}) = \underbrace{\int_{\Gamma} \mathbf{G}_{tu}(\mathbf{x},\mathbf{v};\xi)\mathbf{f}\,\mathrm{d}\Gamma}_{\text{discontinous on }\Gamma} + \int_{\Gamma} \mathbf{G}_{tt}(\mathbf{x},\mathbf{v};\xi,\mathbf{n})(-\mathbf{u})\,\mathrm{d}\Gamma + \int_{\Omega} \left(\mathbf{G}_{tu}^{\alpha,3}(\mathbf{x},\mathbf{v};\xi) - H\,\mathbf{G}_{tq}^{\alpha,\beta}(\mathbf{x},\mathbf{v};\xi)\right)\overline{f}_z(\xi,\eta)\,\mathrm{d}\Omega + \mathbf{N}_x\mathbf{c}\,\overline{f}_z(\xi,\eta) \tag{19}$$

in which $\alpha = 1,2,3;\ \ \beta = 1,2$.

If the plate B is imbedded in the unlimited domain Ω_∞ (Fig. 5), the boundary can be considered both as a boundary $\Gamma = \Gamma^-$ of Ω or boundary Γ^+ of the complementary domain Ω_∞ / Ω; this allows introducing vectors $\mathbf{f}$ and $\mathbf{v}$ defined respectively as "layered forces" and "double-layered displacement jumps" (Fig. 5) (Polizzotto [2]).

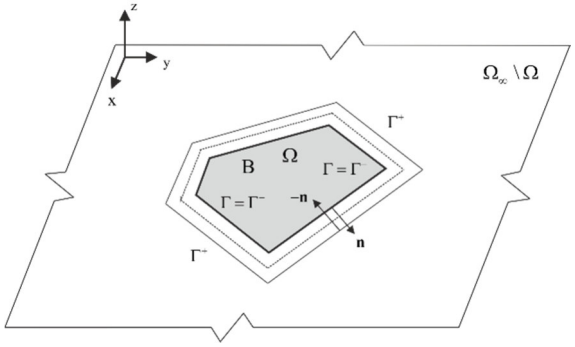

Fig. 5. Plate imbedded in the unlimited domain; boundaries Γ^+ of complementary domain Ω_∞ / Ω and $\Gamma^- = \Gamma$ of the real one.

$$\mathbf{f} = -\mathbf{t}^+ + \mathbf{t}^-; \qquad \mathbf{v} = \mathbf{u}^+ - \mathbf{u}^- \tag{20a, b}$$

In Eqs. (20a, b), $\mathbf{t}^+$, $\mathbf{u}^+$ are traction and displacement vector evaluated on the boundary Γ^+, while $\mathbf{t}^-$, $\mathbf{u}^-$ are the respective vectors on $\Gamma = \Gamma^-$.

The S.I.s of displacements and tractions (18, 19) show discontinuity when $\mathbf{x} \in \Gamma$; if the latter are re-written in symbolic form on the boundary Γ^+ (Fig. 5) it turns out:

$$\mathbf{u}^+ = \mathbf{u}[\mathbf{f}] + \mathbf{u}^{PV}[\mathbf{v}] - \frac{1}{2}\mathbf{u} + \mathbf{u}[\overline{f}_z]; \qquad \mathbf{t}^+ = \mathbf{t}^{PV}[\mathbf{f}] - \frac{1}{2}\mathbf{f} + \mathbf{t}[\mathbf{v}] + \mathbf{t}[\overline{f}_z] \tag{21a, b}$$

In the Eqs. (21a, b) the terms having the apex PV specify that the singular integrals is evaluated as Cauchy Principal Value while the one containing the constant $1/2$ is the associated free terms.

Once the deformation has taken place, the complementary domain Ω_∞ / Ω must be unstressed and undeformed; this means that all strain energy is stored in the plate solid and we write the following conditions, valid at every point of the boundary Γ^+:

$$\mathbf{u}^+ = \mathbf{0}; \qquad \mathbf{t}^+ = \mathbf{0} \tag{22a, b}$$

Eqs. (22a, b) implie that, when the solution is obtained:

$$\mathbf{f} = \mathbf{t}^-; \qquad \mathbf{t}^+ = \mathbf{0} \tag{23a, b}$$

This means that, depending on the constraint conditions, the tractions and displacements must coincide with those originally assigned or with those determined by the analysis.

4. Surface tractions: the RIM technique.

The domain integral in the S.I.s of displacements and tractions (18, 19) are re-written

$$\mathbf{u}[\overline{f}_z] = \int_{\Omega} \left(\mathbf{G}_{uu}^{\alpha,3}(\mathbf{x};\xi) - H\,\mathbf{G}_{uq}^{\alpha,\beta}(\mathbf{x};\xi)\right)\overline{f}_z(\xi,\eta)\,\mathrm{d}\Omega \tag{24}$$

$$\mathbf{t}[\overline{f}_z] = \int_{\Omega} \left(\mathbf{G}_{tu}^{\alpha,3}(\mathbf{x},\boldsymbol{\nu};\xi) - H\,\mathbf{G}_{tq}^{\alpha,\beta}(\mathbf{x},\boldsymbol{\nu};\xi)\right)\overline{f}_z(\xi,\eta)\,\mathrm{d}\Omega + \mathbf{N}_x\,\mathbf{c}\,\overline{f}_z(\xi,\eta) \tag{25}$$

If we put:

$$\mathbf{G}_{uq}^{\alpha,\beta}(\mathbf{x};\boldsymbol{\xi}) = \hat{\mathbf{G}}_{uu}^{\alpha,1}(\mathbf{x};\boldsymbol{\xi}) = \begin{bmatrix} \dfrac{\partial G_{uu}^{1,1}}{\partial \xi} + \dfrac{\partial G_{uu}^{1,2}}{\partial \eta} \\ \dfrac{\partial G_{uu}^{2,1}}{\partial \xi} + \dfrac{\partial G_{uu}^{2,2}}{\partial \eta} \\ \dfrac{\partial G_{uu}^{3,1}}{\partial \xi} + \dfrac{\partial G_{uu}^{3,2}}{\partial \eta} \end{bmatrix}; \quad \mathbf{G}_{tq}^{\alpha,\beta}(\mathbf{x},\boldsymbol{\nu};\boldsymbol{\xi}) = \hat{\mathbf{G}}_{tu}^{\alpha,1}(\mathbf{x},\boldsymbol{\nu};\boldsymbol{\xi}) = \begin{bmatrix} \dfrac{\partial G_{tu}^{1,1}}{\partial \xi} + \dfrac{\partial G_{tu}^{1,2}}{\partial \eta} \\ \dfrac{\partial G_{tu}^{2,1}}{\partial \xi} + \dfrac{\partial G_{tu}^{2,2}}{\partial \eta} \\ \dfrac{\partial G_{tu}^{3,1}}{\partial \xi} + \dfrac{\partial G_{tu}^{3,2}}{\partial \eta} \end{bmatrix} \tag{26a, b}$$

the Eqs. (24, 25) can be written in the form:

$$\mathbf{u}[\bar{f}_z] = \int_{\Omega} \left(\mathbf{G}_{uu}^{\alpha,3}(\mathbf{x};\boldsymbol{\xi}) - H\,\hat{\mathbf{G}}_{uu}^{\alpha,1}(\mathbf{x};\boldsymbol{\xi}) \right) \bar{f}_z(\xi,\eta)\ \mathrm{d}\Omega \tag{27}$$

$$\mathbf{t}[\bar{f}_z] = \int_{\Omega} \left(\mathbf{G}_{tu}^{\alpha,3}(\mathbf{x},\boldsymbol{\nu};\boldsymbol{\xi}) - H\,\hat{\mathbf{G}}_{tu}^{\alpha,1}(\mathbf{x},\boldsymbol{\nu};\boldsymbol{\xi}) \right) \bar{f}_z(\xi,\eta)\,\mathrm{d}\Omega + \mathbf{N}_x\,\mathbf{c}\,\bar{f}_z(\xi,\eta) \tag{28}$$

with $\alpha = 1,2,3$.

In the literature, for $\bar{f}_z(\xi,\eta) = \text{const}$, domain integrals in Eq. (27) involving matrices $\mathbf{G}_{uu}^{\alpha,3}(\mathbf{x};\boldsymbol{\xi})$ and $\hat{\mathbf{G}}_{uu}^{\alpha,1}(\mathbf{x};\boldsymbol{\xi})$ are transformed into boundary integrals, the first one through the use of particular solutions and the second through the divergence theorem (see Weeën [10]); the matrices $\mathbf{G}_{tu}^{\alpha,3}(\mathbf{x},\boldsymbol{\nu};\boldsymbol{\xi})$ e $\hat{\mathbf{G}}_{tu}^{\alpha,1}(\mathbf{x},\boldsymbol{\nu};\boldsymbol{\xi})$ in Eq. (28), suitable for boundary integrals, are obtained through the relationship $\mathbf{t} = (\mathbf{N}_x\,\mathbf{D}\mathbf{C})\mathbf{u}$. The drawback of these operations consists in the fact that any singularity present in the kernel of domain integral reappears in the boundary one; that is, a field of displacements and tractions is obtained continuous within the domain but singular on the boundary Γ (Panzeca [6]).

In order to overcome this drawback, in the present paper, all the domain integrals are transformed into integrals to be performed on the boundary through a general technique. This, valid for any type of law characterizing the surface traction distribution $\bar{f}_z(\xi,\eta)$, provides displacement and traction fields continuous in the domain Ω and without singularities on the boundary Γ .

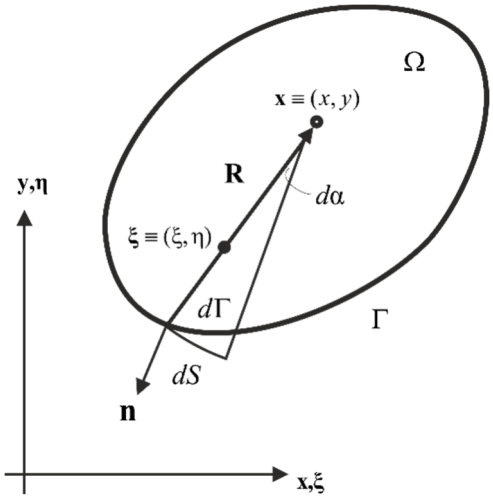

Fig. 6. Scheme for the RIM technique; $\boldsymbol{\xi}$ source point, $\mathbf{x}$ effect point

The technique named Radial Integral Method (RIM), introduced by Gao [24], has been reformulated by Panzeca et al. in [6]; however, in this paper, a simplified formulation of the RIM technique is proposed for domain loads.

The RIM technique (Fig. 6) is applied through the following stages:

- transformation of the integral kernel from the Cartesian coordinate system to a polar one;
- integration with respect to the distance vector $\mathbf{r}$ being $\mathrm{d}\Omega = r\,\mathrm{d}r\,\mathrm{d}\alpha$ and $\mathbf{r} \subseteq \{0, \mathbf{R}\}$; this operation shifts the source point on the boundary;
- transformation to obtain a line integral:

$$\mathbf{R}^2 \partial\alpha = \mathbf{R}\,\mathbf{R}\,\partial\alpha = \mathbf{R}\,\partial S; \qquad \partial S = r_{,n}\,\partial\Gamma \tag{29a, b}$$

- inverse transformation from polar coordinates to Cartesian one.

4.1 RIM technique: fundamental solutions with weak singularities.

The application of the RIM technique to the domain integral present in the S.I. of displacements in Eq. (27) is shown. Let we consider the fundamental solution $G_{uu}^{1,3}(\mathbf{x};\boldsymbol{\xi})$, which exhibits $ln(r)$ singularity; the solution (Appendix 2) is:

$$G_{uu}^{1,3}(\mathbf{x};\boldsymbol{\xi}) = \frac{r\, r_{,x}}{8\pi A}(1-2\,ln(\lambda\, r)) \tag{30}$$

The phases of the RIM technique for $\overline{f}_z(\boldsymbol{\xi},\eta) = \text{const}$ allow writing:

$$\begin{aligned}\int_0^{2\pi}\int_0^R G_{uu}^{1,3}(\varphi)\, r\, \mathrm{d}r\, \mathrm{d}\alpha\, \overline{f}_z &= \int_0^{2\pi}\int_0^R \left(\frac{r\cos(\alpha)}{8A\pi}(1-2\,ln(\lambda\, r))\right) r\, \mathrm{d}r\, \mathrm{d}\alpha\, \overline{f}_z = \int_0^{2\pi}\left(\frac{r\cos(\alpha)(5-6\,ln(\lambda\, r))}{72A\pi}\right) r^2\, \mathrm{d}\alpha\, \overline{f}_z = \\ &= \int_{\Gamma_s}\left(\frac{r_x(5-6\,ln(\lambda\, r))}{72A\pi}\right) r\, \mathrm{d}S\, \overline{f}_z = \int_{\Gamma}\left(\frac{r_x(5-6\,ln(\lambda\, r))}{72A\pi}\right) r\, r_{,n}\, \mathrm{d}\Gamma\, \overline{f}_z\end{aligned} \tag{31}$$

It turns out

$$G_{uu}^{1,3\text{-}B}(\mathbf{x};\boldsymbol{\xi}) = \frac{r_x(5-6\,ln(\lambda r))}{72A\pi} r\, r_{,n} \tag{32}$$

where the apex B characterizes that the solution is suitable for boundary integration.
It is important to note that the normal derivative $r_{,n}$ present in Eq. (32) implies that $G_{uu}^{1,3\text{-}B}(\mathbf{x};\boldsymbol{\xi}) = 0$ when $\mathbf{x} \equiv \boldsymbol{\xi}$ inasmuch as $\mathbf{n} \perp \mathbf{r}$ on the boundary Γ; we obtain a regular field of displacements inside the domain and null on the boundary.
In the same way, the technique also applies to fundamental solutions $\mathbf{G}_{tu}^{\alpha,3}(\mathbf{x},\boldsymbol{\nu};\boldsymbol{\xi})$ and $\hat{\mathbf{G}}_{uu}^{\alpha,1}(\mathbf{x};\boldsymbol{\xi})$ which show singularities of order r^{-1}. The fundamental solutions matrices $\mathbf{G}_{uu}^{\alpha,3-B}(\mathbf{x};\boldsymbol{\xi})$, $\mathbf{G}_{tu}^{\alpha,3-B}(\mathbf{x},\boldsymbol{\nu};\boldsymbol{\xi})$, $\hat{\mathbf{G}}_{uu}^{\alpha,1-B}(\mathbf{x};\boldsymbol{\xi})$ suitable for integrations on the boundar y for $\overline{f}_z(\boldsymbol{\xi},\eta) = \text{const}$ are given in Appendix 2.

4.2 RIM technique: fundamental solutions with hypersingularities.

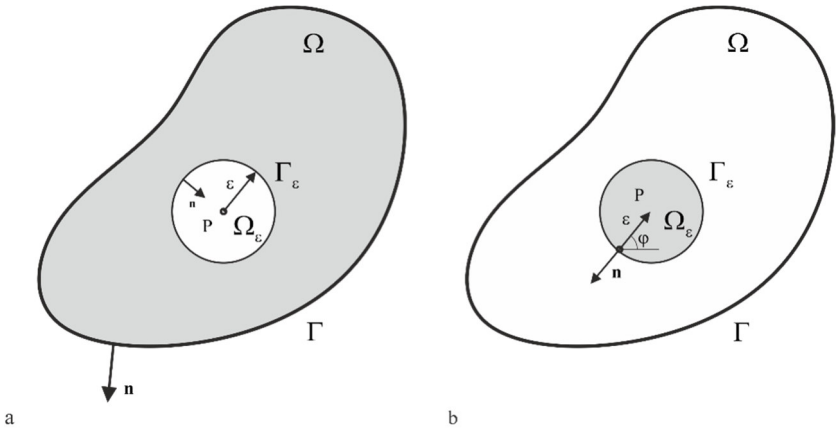

Fig. 7. Zenith view of the plate subjected to the force $\overline{f}_z$ applied at P : a) domain $\Omega - \Omega_\varepsilon$, b) circular domain Ω_ε of exclusion with radius ε and boundary Γ_ε for the Bui Free Term evaluation.

The application of the RIM technique to the domain integral present in the S.I. of tractions (28), since the fundamental solution $\hat{\mathbf{G}}_{tu}^{\alpha,1}(\mathbf{x},\boldsymbol{\nu};\boldsymbol{\xi})$ exhibits hypersingularity of order r^{-2}, applies through a regularization strategy (see Panzeca [6]).
The regularization technique begins from the S.I. of the displacements Eq. (27) here re-written for $\overline{f}_z(\boldsymbol{\xi},\eta) = \text{const}$:

$$\mathbf{u}[\overline{f}_z] = -H\int_\Omega \hat{\mathbf{G}}_{uu}^{\alpha,1}(\mathbf{x};\boldsymbol{\xi})\, \mathrm{d}\Omega\, \overline{f}_z \tag{33}$$

Starting from Eq. (33) and applying $\mathbf{t} = (\mathbf{N}_x\, \mathbf{D}\mathbf{C})\mathbf{u}$ we write:

$$\mathbf{t}[\overline{f}_z] = -H\, \mathbf{N}_x\, \mathbf{D}\mathbf{C}_x \int_\Omega \hat{\mathbf{G}}_{uu}^{\alpha,1}(\mathbf{x};\boldsymbol{\xi})\, \mathrm{d}\Omega\, \overline{f}_z + H\, \mathbf{N}_x \mathbf{c}\, \overline{f}_z \tag{34}$$

With reference to Fig. 7a the domain integral in Eq. (34) may be rewritten as follows:

$$-H\,\mathbf{N}_x\mathbf{D}\mathbf{C}_x\int_{\Omega}\hat{\mathbf{G}}^{\alpha,1}_{uu}(\mathbf{x};\boldsymbol{\xi})\,\mathrm{d}\Omega\,\overline{f}_z=-H\left(\mathbf{N}_x\mathbf{D}\lim_{\varepsilon\to 0}\int_{\Omega-\Omega_\varepsilon}\mathbf{C}_x\hat{\mathbf{G}}^{\alpha,1}_{uu}(\mathbf{x};\boldsymbol{\xi})\,\overline{f}_z\,\mathrm{d}\Omega+\mathbf{N}_x\mathbf{D}\lim_{\varepsilon\to 0}\int_{\Omega_\varepsilon}\mathbf{C}_x\hat{\mathbf{G}}^{\alpha,1}_{uu}(\mathbf{x};\boldsymbol{\xi})\,\mathrm{d}\Omega\,\overline{f}_z\right) \tag{35}$$

The first integral to the right in Eq. (35) is evaluated as CPV and can be written as

$$\mathbf{N}_x\mathbf{D}\lim_{\varepsilon\to 0}\int_{\Omega-\Omega_\varepsilon}\mathbf{C}_x\hat{\mathbf{G}}^{\alpha,1}_{uu}(\mathbf{x};\boldsymbol{\xi})\,\overline{f}_z\mathrm{d}\Omega=\int_{\Omega}\hat{\mathbf{G}}^{\alpha,1}_{tu}(\mathbf{x},\boldsymbol{\nu};\boldsymbol{\xi})(f_z-\overline{f}_z)\,\mathrm{d}\Omega+\lim_{\varepsilon\to 0}\int_{\Omega-\Omega_\varepsilon}\hat{\mathbf{G}}^{\alpha,1}_{tu}(\mathbf{x},\boldsymbol{\nu};\boldsymbol{\xi})\mathrm{d}\Omega\,\overline{f}_z \tag{36}$$

where a singularity arises in the second integral of the right of the previous expression Eq. (36).
This latter domain singular integral is transformed into an integral to be computed on the boundary through the application of the RIM technique. We obtain:

$$\lim_{\varepsilon\to 0}\int_{\Omega-\Omega_\varepsilon}\hat{\mathbf{G}}^{\alpha,1}_{tu}(\mathbf{x},\mathbf{v};\boldsymbol{\xi})\,\overline{f}_z\,\mathrm{d}\Omega=\int_{\Gamma}\hat{\mathbf{G}}^{\alpha,1-B}_{tu}(\mathbf{x},\mathbf{v};\boldsymbol{\xi},\mathbf{n})\,\overline{f}_z\,\mathrm{d}\Gamma \tag{37}$$

The second integral on the right of Eq. (35), through the condition $\mathbf{C}_x(\cdot)=-\mathbf{C}_\xi(\cdot)$ and the use of the Gauss Theorem, is transformed into an integral defined on the boundary Γ_ε (Fig. 7b), thus making it possible to define the Bui Free Term. After the transformation of the variable from Cartesian into polar ones, the latter integral is evaluated in closed form as follows:

$$\mathbf{J}=\lim_{\varepsilon\to 0}\int_{\Omega_\varepsilon}\mathbf{C}_x\hat{\mathbf{G}}^{\alpha,1}_{uu}(\mathbf{x};\boldsymbol{\xi})\,\mathrm{d}\Omega_z=-\lim_{\varepsilon\to 0}\int_{\Omega_\varepsilon}\mathbf{C}_\xi\hat{\mathbf{G}}^{\alpha,1}_{uu}(\mathbf{x};\boldsymbol{\xi})\,\mathrm{d}\Omega)=-\int_{\Gamma_\varepsilon}\mathbf{N}_\xi\hat{\mathbf{G}}^{\alpha,1}_{uu}(\mathbf{x};\boldsymbol{\xi})\,\mathrm{d}\Gamma_\varepsilon=\int_{\Gamma_\varepsilon}\mathbf{N}_\varphi\frac{\tilde{\boldsymbol{\Psi}}^{\alpha,1}_{uu}(\varphi)}{\varepsilon}\varepsilon\,\mathrm{d}\Gamma_\varepsilon=\frac{1}{2A}\mathbf{w} \tag{38}$$

where $\mathbf{w}^T=[1,1,0]^T$. The vector $\mathbf{J}$ is the Bui Free Term for the Reissner's model.
Finally, the regularized S.I. of traction is obtained:

$$\begin{aligned}\mathbf{t}(\mathbf{x},\mathbf{v};\boldsymbol{\xi},\boldsymbol{\eta})=&\int_{\Gamma}\mathbf{G}_{tu}(\mathbf{x},\mathbf{v};\boldsymbol{\xi})\mathbf{f}\,\mathrm{d}\Gamma+\int_{\Gamma}\mathbf{G}_{tt}(\mathbf{x},\mathbf{v};\boldsymbol{\xi},\mathbf{n})(-\mathbf{u})\,\mathrm{d}\Gamma-H\int_{\Omega}\hat{\mathbf{G}}^{\alpha,1}_{tu}(\mathbf{x},\boldsymbol{\nu};\boldsymbol{\xi})(f_z-\overline{f}_z)\,\mathrm{d}\Omega+\\&+\int_{\Gamma}\left(\mathbf{G}^{\alpha,3-B}_{tu}(\mathbf{x},\mathbf{v};\boldsymbol{\xi},\mathbf{n})-H\,\hat{\mathbf{G}}^{\alpha,1-B}_{tu}(\mathbf{x},\mathbf{v};\boldsymbol{\xi},\mathbf{n})\right)\overline{f}_z\,\mathrm{d}\Gamma-H\,\mathbf{N}_x(\mathbf{D}\mathbf{J}-\mathbf{g})\overline{f}_z\end{aligned} \tag{39}$$

where

$$\mathbf{D}\mathbf{J}=\left[\frac{1+\nu}{2}\quad\frac{1+\nu}{2}\quad 0\quad 0\quad 0\right]^T \tag{40}$$

$$(\mathbf{D}\mathbf{J}-\mathbf{g})=\left[-\frac{1-\nu}{2}\quad-\frac{1-\nu}{2}\quad 0\quad 0\quad 0\right]^T \tag{41}$$

$$\mathbf{N}_x(\mathbf{D}\mathbf{J}-\mathbf{g})=\left[-\left(\frac{1-\nu}{2}\right)\nu_x\quad-\left(\frac{1-\nu}{2}\right)\nu_y\quad 0\quad 0\quad 0\right]^T. \tag{42}$$

and $\mathbf{g}^T=[1,1,0,0,0]$.
The RIM technique provides also the transformed regularized domain integral in Eq. (39); this results is null since $\overline{f}_z$ is constant on the entire domain; we obtain a regular field of tractions inside the domain and null on the boundary.
Appendix 2 provide the matrix $\hat{\mathbf{G}}^{\alpha,1-B}_{tu}(\mathbf{x},\boldsymbol{\nu};\boldsymbol{\xi})$.

5. Solving system by the "progenitor matrix"

The solving system within the SGBEM is obtained through an indirect approach based on the generation of a matrix called "progenitor matrix" introduced by Terravecchia [27] in order to operate a generalization of the analysis method without distinguishing initially the effective boundary conditions. The "progenitor matrix" allows obtaining all the coefficients of the solving system and the boundary load vectors.
The stages of the approach are:

- the plate is imbedded in an unlimited domain having the same physical and mechanical characteristics; this allows recognizing a complementary domain $\Omega_\infty\setminus\Omega$ of boundary Γ^+ and a real domain Ω of boundary $\Gamma\equiv\Gamma^-$ (Fig. 5);

- imposition on the boundary Γ^+ of the conditions (22a, b) here re-written:

$$\mathbf{u}^+(\mathbf{x}) = \mathbf{0}; \quad \mathbf{t}^+(\mathbf{x}, \boldsymbol{\nu}) = \mathbf{0} \tag{43a, b}$$

- boundary discretization and modelling of the quantities $\mathbf{u}$ and $\mathbf{f}$ as a function of the nodal quantities $\mathbf{F}$ and $\mathbf{V} = -\mathbf{U}$:

$$\mathbf{f} = \boldsymbol{\psi}_t \mathbf{F}; \quad \mathbf{u} = \boldsymbol{\psi}_u \mathbf{V} \tag{44a, b}$$

where $\boldsymbol{\psi}_t$ and $\boldsymbol{\psi}_u$ are suitable diagonal matrices of shape functions;

- introduction of modelling (44a, b) in the S.I.s (18, 19) written on the boundary Γ^+ with $\bar{f}_z = \text{const}$:

$$\mathbf{u}^+ = \int_{\Gamma^+} \mathbf{G}_{uu} \boldsymbol{\psi}_t \mathbf{F}\, \mathrm{d}\Gamma + \oint_{\Gamma^+} \mathbf{G}_{ut} \boldsymbol{\psi}_u \mathbf{V} \mathrm{d}\Gamma + \frac{1}{2} \mathbf{I} \boldsymbol{\psi}_u \mathbf{V} + \int_{\Gamma^+} \left(\mathbf{G}_{uu}^{\alpha,3-B} - H \tilde{\mathbf{G}}_{uq}^{\alpha,1-B} \right) \bar{f}_z \, \mathrm{d}\Gamma \tag{45}$$

$$\mathbf{t}^+ = \oint_{\Gamma^+} \mathbf{G}_{tu} \boldsymbol{\psi}_t \mathbf{F} \mathrm{d}\Gamma - \frac{1}{2} \mathbf{I} \boldsymbol{\psi}_t \mathbf{F} + \int_{\Gamma^+} \mathbf{G}_{tt} \boldsymbol{\psi}_u \mathbf{V} \, \mathrm{d}\Gamma + \int_{\Gamma^+} \left(\mathbf{G}_{tu}^{\alpha,3-B} - H \tilde{\mathbf{G}}_{tq}^{\alpha,1-B} \right) \bar{f}_z \, \mathrm{d}\Gamma - H \, \mathbf{N}_x (\mathbf{D}\mathbf{J} - \mathbf{g}) \bar{f}_z \tag{46}$$

- weighing, according to the Galerkin strategy, of the boundary conditions (43a, b) using dual shape functions in an energetic sense:

$$\mathbf{W}^+ = \int_{\Gamma^+} \boldsymbol{\psi}_t \, \mathbf{u}^+ \mathrm{d}\Gamma = \mathbf{0}; \quad \mathbf{P}^+ = \int_{\Gamma^+} \boldsymbol{\psi}_u \, \mathbf{t}^+ \mathrm{d}\Gamma = \mathbf{0} \tag{47a, b}$$

- replacement of S.I.s Eqs. (45, 46) in Eqs. (47a, b) and generation of the matrix relation:

$$\begin{bmatrix} \mathbf{W}^+ \\ \mathbf{P}^+ \end{bmatrix} = \begin{bmatrix} \mathbf{A}_{uu} & \mathbf{A}_{ut} + \mathbf{C}_{ut} \\ \mathbf{A}_{tu} - \mathbf{C}_{tu} & \mathbf{A}_{tt} \end{bmatrix} \cdot \begin{bmatrix} \mathbf{F} \\ \mathbf{V} \end{bmatrix} + \begin{bmatrix} \mathbf{W}_\Omega^+ \\ \mathbf{P}_\Omega^+ \end{bmatrix} \bar{f}_z = \begin{bmatrix} \mathbf{0} \\ \mathbf{0} \end{bmatrix} \tag{48}$$

where

$$\begin{aligned}
&\mathbf{A}_{uu} = \int_{\Gamma^+} \boldsymbol{\psi}_t \left(\int_{\Gamma^+} \mathbf{G}_{uu} \boldsymbol{\psi}_t \mathrm{d}\Gamma \right) \mathrm{d}\Gamma; \quad && \mathbf{A}_{ut} = \int_{\Gamma^+} \boldsymbol{\psi}_t \left(\oint_{\Gamma^+} \mathbf{G}_{ut} \boldsymbol{\psi}_u \mathrm{d}\Gamma \right) \mathrm{d}\Gamma \\
&\mathbf{A}_{tu} = \int_{\Gamma^+} \boldsymbol{\psi}_u \left(\oint_{\Gamma^+} \mathbf{G}_{tu} \boldsymbol{\psi}_t \mathrm{d}\Gamma^+ \right) \mathrm{d}\Gamma; \quad && \mathbf{A}_{tt} = \int_{\Gamma^+} \boldsymbol{\psi}_u \left(\int_{\Gamma^+} \mathbf{G}_{tt} \boldsymbol{\psi}_u \mathrm{d}\Gamma \right) \mathrm{d}\Gamma \\
&\mathbf{C}_{tu} = \frac{1}{2} \int_{\Gamma^+} \boldsymbol{\psi}_u \boldsymbol{\psi}_t \mathrm{d}\Gamma; \quad && \mathbf{C}_{ut} = \frac{1}{2} \int_{\Gamma^+} \boldsymbol{\psi}_t \boldsymbol{\psi}_u \mathrm{d}\Gamma \\
&\mathbf{W}_\Omega^+ = \int_{\Gamma^+} \boldsymbol{\psi}_t (\mathbf{u}[\bar{f}_z]) \mathrm{d}\Gamma; \quad && \mathbf{P}_\Omega^+ = \int_{\Gamma^+} \boldsymbol{\psi}_u (\mathbf{u}[\bar{f}_z]) \mathrm{d}\Gamma
\end{aligned} \tag{49a-h}$$

Since the symmetry properties Eqs. (11, 12) are valid, it turns out:

$$\mathbf{A}_{uu} = \mathbf{A}_{uu}^T; \quad \mathbf{A}_{tt} = \mathbf{A}_{tt}^T; \quad \mathbf{A}_{tu} = \mathbf{A}_{ut}^T; \quad \mathbf{C}_{tu} = \mathbf{C}_{ut}^T. \tag{50a-d}$$

Eq. (48), with obvious meaning of symbols, is rewritten in the form:

$$\begin{bmatrix} \mathbf{W}^+ \\ \mathbf{P}^+ \end{bmatrix} = \begin{bmatrix} \mathbf{B}_{uu} & \mathbf{B}_{ut} \\ \mathbf{B}_{tu} & \mathbf{B}_{tt} \end{bmatrix} \cdot \begin{bmatrix} \mathbf{F} \\ \mathbf{V} \end{bmatrix} + \begin{bmatrix} \mathbf{W}_\Omega^+ \\ \mathbf{P}_\Omega^+ \end{bmatrix} \bar{f}_z = \begin{bmatrix} \mathbf{0} \\ \mathbf{0} \end{bmatrix} \tag{51}$$

in which $\mathbf{B}$ is the "progenitor matrix" of the analysed plate and it is non-symmetric and non-invertible. It is possible to check coefficient blocks $\mathbf{B}_{ut}$, $\mathbf{B}_{tt}$ through rigid body motion techniques and check coefficient block $\mathbf{B}_{uu}$ through a technique of superimposing effects (Terravecchia [27]).

- imposition of the effective boundary conditions on $\Gamma = \Gamma_1 + \Gamma_2$ and distinction of known and unknown quantities

$$\mathbf{F}^T = \left[\bar{\mathbf{F}}_2 \quad \mathbf{F}_1\right]^T; \quad \mathbf{V}^T == \left[\mathbf{V}_2 \quad \bar{\mathbf{V}}_1\right]^T = \left[-\mathbf{U}_2 \quad -\bar{\mathbf{U}}_1\right]^T \tag{52a, b}$$

resulting in the reordering and partitioning of the progenitor matrix and of the domain load vector:

$$\left[\begin{array}{c} \mathbf{W}_2^+ = \mathbf{0} \\ \hline \mathbf{W}_1^+ = \mathbf{0} \\ \mathbf{P}_2^+ = \mathbf{0} \\ \hline \mathbf{P}_1^+ = \mathbf{0} \end{array}\right] = \left[\begin{array}{c|cc|c} \mathbf{B}_{u2u2} & \mathbf{B}_{u2u1} & \mathbf{B}_{u2t2} & \mathbf{B}_{u2t1} \\ \hline \mathbf{B}_{u1u2} & \mathbf{B}_{u1u1} & \mathbf{B}_{u1t2} & \mathbf{B}_{u1t1} \\ \mathbf{B}_{t2u2} & \mathbf{B}_{t2u1} & \mathbf{B}_{t2t2} & \mathbf{B}_{t2t1} \\ \hline \mathbf{B}_{t1u2} & \mathbf{B}_{t1u2} & \mathbf{B}_{t1t2} & \mathbf{B}_{t1t1} \end{array}\right] \cdot \left[\begin{array}{c} \bar{\mathbf{F}}_2 \\ \hline \mathbf{F}_1 \\ \mathbf{V}_2 \\ \hline \bar{\mathbf{V}}_2 \end{array}\right] + \left[\begin{array}{c} \mathbf{W}_{2\Omega}^+ \\ \hline \mathbf{W}_{1\Omega}^+ \\ \mathbf{P}_{2\Omega}^+ \\ \hline \mathbf{P}_{1\Omega}^+ \end{array}\right] \tag{53}$$

- taking the matrix of the solving system and the load vectors:

$$\left[\begin{array}{cc} \mathbf{B}_{u1u1} & \mathbf{B}_{u1t2} \\ \mathbf{B}_{t2u1} & \mathbf{B}_{t2t2} \end{array}\right] \cdot \left[\begin{array}{c} \mathbf{F}_1 \\ \mathbf{V}_2 \end{array}\right] + \left[\begin{array}{c} \mathbf{B}_{u1u2} \\ \mathbf{B}_{t2u2} \end{array}\right] \cdot \bar{\mathbf{F}}_2 + \left[\begin{array}{c} \mathbf{B}_{u1t1} \\ \mathbf{B}_{t2u2} \end{array}\right] \cdot \bar{\mathbf{V}}_2 + \left[\begin{array}{c} \mathbf{W}_{1\Omega}^+ \\ \mathbf{P}_{2\Omega}^+ \end{array}\right] \cdot \bar{f}_z \tag{54}$$

Eq. (54) is re-written in the form:

$$\mathbf{K}\,\mathbf{X} + \mathbf{L}_t \bar{\mathbf{F}}_2 + \mathbf{L}_u \bar{\mathbf{V}}_1 + \mathbf{L}_\Omega = \mathbf{0} \tag{55}$$

where $\mathbf{K}$ is the symmetric and defined pseudostiffness matrix of the system and $\mathbf{L}_t$, $\mathbf{L}_u$, $\mathbf{L}_\Omega$ are respectively the load vectors of boundary traction $\bar{\mathbf{F}}_2$, boundary double-layered displacements $\bar{\mathbf{V}}_2$ and domain tractions $\bar{f}_z$.
Basically, the indirect approach makes available a matrix of coefficients on which it is possible to impose the actual boundary conditions thus being able to consider a wide range of loading possibilities. In Eq. (53) the rows of weighted displacements and tractions $\mathbf{W}_2^+ = \mathbf{0}$ and $\mathbf{P}_1^+ = \mathbf{0}$, not verified by solution, are available for further post-analysis steps such as: improvement of discretization on the boundary through the evaluation of weighted residuals or energy considerations [28]; energy evaluation in the body domain and in the unlimited domain [29].

5.1 Hypersingular coefficient calculation.

The matrix $\mathbf{A}_{tt}$, when $\mathbf{x} \equiv \boldsymbol{\xi}$, is characterized by double integrals with r^{-2} order of singularity. In this paper, the kernel of the hypersingular integral is interpreted as a distribution (Terravecchia [4]); this allows computing the integral, independently of asymptotic behaviour of the function. This operation take on a strong physical meaning: the inner integral permits to obtain a function defining the response at every point of the infinite domain Ω_∞, the external one performs the weighting of the effect on the body boundary; the technique is applied through a decomposition of the causes and a superimposition of the effects.
Let's calculate (Fig. 8) coefficient showing hypersingularity in the case of two aligned boundary elements a and b the length of which is indicated respectively with a and b. It takes into account the fundamental solution $G_{tt}^{I,I}$ provided in the Appendix 2; the latter permits to obtain, in the unlimited domain Ω_∞, the moments M_{nx} caused by double-layered rotations $\mathrm{v}_x = -\varphi_x$ both referred to the general system introduced in Fig. 1; in this case, the above quantities assume respectively the meaning of moments and distortions of torsional type. By using the power series expansion of the Bessel function (Appendix 1), we divide the $G_{tt}^{I,I}$ fundamental solution into a singular part $G_{tt}^{I,I-S}$ and a regular part $G_{tt}^{I,I-R}$. The regular part does not require particular treatments and the double integral is performed through numerical integration techniques; the singular part is treated through the theory of distributions.
If we apply the power series expansion of the Bessel functions, the singular part $G_{tt}^{I,I-S}$ takes the form:

$$G_{tt}^{I,I-S} = -\frac{A(1-n)\lambda^2}{8\pi}\left[(r_{,n}r_{,\nu} + r_{,t}r_{,\tau})\,ln\left(\frac{z}{2}\right) + \frac{2(1+n)}{z^2}(2r_{,x}r_{,y}(r_{,t}r_{,\nu} + r_{,n}r_{,\tau}) + (r_{,n}, r_{,\nu} + r_{,t}r_{,\tau}) - 4r_{,x}^2 r_{,n}r_{,\nu}\right] \tag{56}$$

Eq. (56), simplified through the data that characterize the position of the boundary elements a and b (Fig. 8) i.e.

$$\{y = 0,\ v_x = 0,\ v_y = 1,\ \eta = 0,\ n_x = 0,\ n_y = 1\} \tag{57}$$

turns out:

$$G_{tt}^{I,I-S} = m_{nx}^{*} = \frac{A(1-n)\lambda^2}{8\pi}\left[\frac{2(1+n)}{r_x^2\lambda^2} + ln\left(\frac{r_x\lambda}{2}\right)\right] \tag{58}$$

Into the Eq. (58) it is noted that the weak singularity and hypersingularity concern all the support of the boundary elements. The shape functions used for cause modelling and effect weighting, indicated by subscripts respectively c and e are of linear type:

$$\psi_{ac} = 1+\frac{\xi}{a};\quad \psi_{ae} = 1+\frac{x}{a};\quad \psi_{bc} = 1-\frac{\xi}{b};\quad \psi_{be} = 1-\frac{x}{b} \tag{59a-d}$$

and the nodal value of the cause in the common node N is $V_x = 1$.

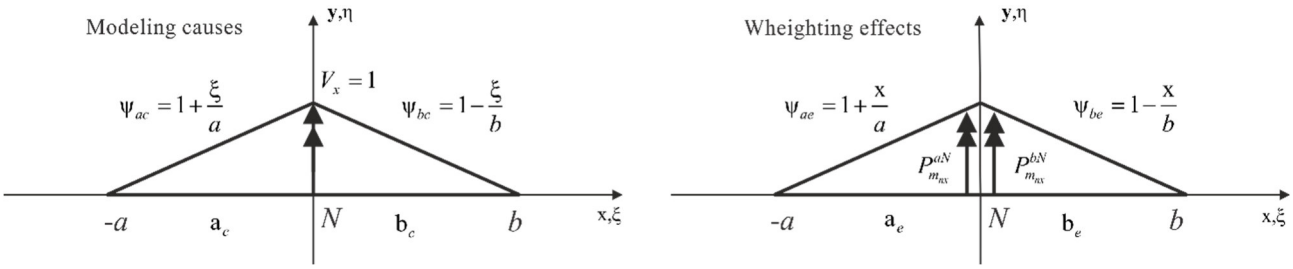

Fig. 8. Scheme of hypersingular coefficient calculation.

By decomposing the causes and superimposing the effects, we write:

$$P_{nx}^{N} = P_{nx}^{aN} + P_{nx}^{bN} = \int_{\Gamma_{ae}} \psi_{ae}\Big(\underbrace{\int_{\Gamma_{ac}} m_{nx}^{*}\psi_{ac}\,d\Gamma_{ac}}_{m_{nx}^{aa}} + \underbrace{\int_{\Gamma_{bc}} m_{nx}^{*}\psi_{bc}\,d\Gamma_{bc}}_{m_{nx}^{ab}}\Big)d\Gamma_{ae} + \int_{\Gamma_{ae}} \psi_{be}\Big(\underbrace{\int_{\Gamma_{ac}} m_{nx}^{*}\psi_{ac}\,d\Gamma_{ac}}_{m_{nx}^{ba}} + \underbrace{\int_{\Gamma_{bc}} m_{nx}^{*}\psi_{bc}\,d\Gamma_{bc}}_{m_{nx}^{bb}}\Big)d\Gamma_{be} \tag{60}$$

$$\underbrace{\qquad\qquad\qquad\qquad\qquad\qquad}_{m_{nx}^{a}} \qquad\qquad \underbrace{\qquad\qquad\qquad\qquad\qquad\qquad}_{m_{nx}^{b}}$$

In Eq. (60) the terms m_{nx}^{aa} and m_{nx}^{ab}, defining the response m_{nx}^{a} at every point of boundary element a for applied causes respectively to a and b, show singularities r^{-1} of opposite sign which cancel each other out in the sum; logarithmic singularities add up and in the weighing process will be eliminated through an integration by parts (Terravecchia [4]). This leads to the calculation of the P_{nx}^{a} part of the coefficient. Similar considerations concern the part P_{nx}^{b}.

The total value P_{nx}^{N} of the weighted moment associated with the node N is:

$$P_{nx}^{N} = \frac{A(1-n)\lambda^2}{8\pi}\frac{(a+b)}{12ab}\left[\begin{array}{l}\dfrac{24(1+n)}{\lambda^2}((a+b)ln(a+b)-a\,ln(a)-b\,ln(b)) + \dfrac{25\,ab}{4}(a+b) - 3ab(a+b)ln\left(\dfrac{\lambda}{2}\right) + \\ -ab(a\,ln(a)+b\,ln(b)) - (a+b)^3 ln(a+b) + (a+b)(a^2\,ln(a)+b^2\,ln(b))\end{array}\right] \tag{61}$$

6. Post analysis phase.

The calculated response on the boundary Γ, in terms of nodal traction $\mathbf{F}_1$ and nodal displacements $-\mathbf{U}_2$, allows obtaining the distribution of tractions and displacements on the boundary by modelling them through nodal values:

$$\mathbf{t}_1 = \boldsymbol{\psi}_t\,\mathbf{F}_1;\qquad \mathbf{u}_2 = \boldsymbol{\psi}_u\,\mathbf{U}_2 \tag{62}$$

The displacements and tractions at the internal points of the domain are obtained through S.I.s (18, 19) where all quantities are now known.

The internal stress, since the bending and shear stresses are assumed to vary linearly and quadratic respectively, are achieved through relationships

$$\boldsymbol{\sigma} = \frac{12\,z}{h^3}\mathbb{m};\qquad \boldsymbol{\tau} = \frac{3\,z}{2\,h}\left[1-4\left(\frac{z}{h}\right)^2\right]\mathbb{t}; \tag{63a, b}$$

with $\mathbb{m}, \mathbb{t}$ evaluated through the S.I.s. (16); the stress σ_z is given by the Eq. (4).

The plate's equilibrium subjected to vertical loads is:

$$\sum_i \int_{\Gamma_i} \boldsymbol{\psi}_t\,\mathbf{T}_n\,d\Gamma_i = \sum_i \int_{\Gamma_i} \boldsymbol{\psi}_t\,\bar{\mathbf{T}}_n\,d\Gamma_i + \int_{\Omega} \bar{f}_z\,d\Omega \tag{64}$$

where $\mathbf{T}_n$, $\overline{\mathbf{T}}_n$ are the reactive and active vertical nodal forces, respectively and $\overline{f}_z$ the domain vertical loads.
The check of Eq. (64) is index of the goodness of the solution.

7. Numerical examples.

The numerical examples deal with problems for which the analytical solution is known. Examples are solved using the "progenitor matrix" approach. For certain physical and geometric characteristics, a matrix of coefficients is made available which, reordered on the basis of the effective boundary conditions, allows simulating a multiplicity of load conditions. Rigid body motion techniques, since the internal displacement and traction fields are known, allowing determine the optimal number of terms in the series expansion of the Bessel functions (see Appendix 1) to be considered in the coefficients calculation of the progenitor matrix. For the following examples, thirty terms of the power series expansion give very good results; in fact, the internal displacement and traction fields expected from rigid body motion techniques are well approximated and allow the numerical precision of the machine to be achieved.
The results of the examples are provided in both tables and graphs. In the table, the tractions on the constrained nodes and the displacements of the free nodes, obtained in the analysis phase, are compared with the analytical solution. The dashed lines in the tables indicate that the solution cannot be provided either by the analytical solution or by the solution through SGBEM: i.e. displacements of the constrained nodes or tractions of the free nodes. This avoids the proliferation of results tables.

7.1 Example 1: square plate in pure torsion, with angle of torsion $\theta = 1$.

Let us consider the square plate of Fig. 9a having dimensions, $L \times L = 2 \times 2$, $h = 1$ and $\lambda = \sqrt{10}$; to simplify the calculations, the adopted physical characteristics are, Young's modulus $E = 12$, Poisson ratio $n = 0$ which results in a bending stiffness $A = 1$.
The plate is discretized by 8 quadratic boundary elements for a total of 16 nodes on the boundary; lowercase letters indicate the sides of the plate on which the boundary conditions are imposed. The entire "progenitor matrix" is calculated which, in order to show the potential of the approach, will also be used for Example 2.
The results obtained are also compared with those obtained in [20] introduced in suitable tables.

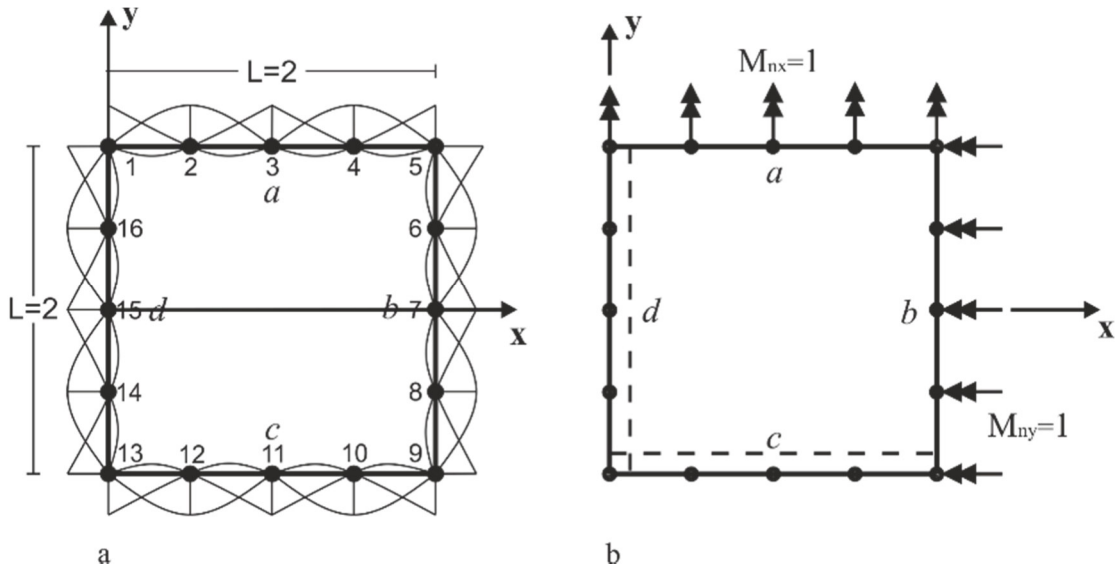

Fig. 9. Square plate a) discretized by 8 quadratic boundary elements, b) boundary load in pure torsion.

The plate (Fig. 9b), simply supported on sides *c*, *d* with boundary conditions

$$\left[\overline{\varphi}_x = 0, \overline{u}_z = 0, \overline{M}_{ny} = 0\right] \text{ on } c; \quad \left[\overline{\varphi}_y = 0, \overline{u}_z = 0, \overline{M}_{nx} = 0\right] \text{ on } d \tag{65a, b}$$

is subjected on the free side *a*, *b* to a distribution of twisting moments which take on a unitary value i.e.

$$\overline{M}_{nx} = \overline{M}_{ny} = A(1-n)\theta = 1 \tag{66a, b}$$

The analytical solution of this problem is [20]

$$\varphi_x = \theta(y + L/2), \quad \varphi_y = \theta x, \quad u_z = -\theta xy\,. \tag{67a-c}$$

Present approach						
Node	**Analytical solution**			**SGBEM – 8 quadratic elements**		
	M_{nx}	M_{ny}	T_n	M_{nx}	M_{ny}	T_n
9	-1.00000	$---$	0	-1.00000	$---$	1×10^{-4}
10	-1.00000	$---$	0	-0.99997	$---$	-5×10^{-5}
11	-1.00000	$---$	0	-1.00002	$---$	8×10^{-5}
12	-1.00000	$---$	0	-0.99997	$---$	-4×10^{-5}
13	-1.00000	-1.00000	0	-1.00002	-1.00002	8×10^{-5}
14	$---$	-1.00000	0	$---$	-0.99997	-4×10^{-5}
15	$---$	-1.00000	0	$---$	-1.00002	8×10^{-5}
16	$---$	-1.00000	0	$---$	-0.99997	-5×10^{-5}
1	$---$	-1.00000	0	$---$	-1.00000	1×10^{-4}

Table EI a. Example 1: tractions, analytical and SGBEM solution.

Reference [20]						
	Analytical solution		**SGBEM - 16 quadratic elements**		**SGBEM - 32 quadratic elements**	
	M_{nx}	T_n	M_{nx}	T_n	M_{nx}	T_n
9	-1.000	0.0	-1.191	-0.025	-1.148	-0.025
10	-1.000	0.0	-1.045	0.019	-1.015	0.007
11	-1.000	0.0	-1.055	-0.024	-1.017	0.001
12	-1.000	0.0	-1.028	0.017	-1.032	-0.014
13	-1.000	0.0	-1.104	-0.165	-1.071	-0.128

Table EI b. Example 1: tractions, analytical and SGBEM solution in reference [20].

Present approach						
Node	**Analytical solution**			**SGBEM – 8 quadratic elements**		
	φ_x	φ_y	u_z	φ_x	φ_y	u_z
1	2	0	0	2.00001	$---$	$---$
2	2	0.5	-1	2.00001	0.50008	-1.00001
3	2	1	-2	2.00001	1.00001	-2.00001
4	2	1.5	-3	2.00001	1.50001	-3.00001
5	2	2	-4	2.00001	2.00001	-4.00002
6	1.5	2	-3	1.50001	2.00001	-3.00001
7	1	2	-2	1.00001	2.00001	-2.00001
8	0.5	2	-1	0.50008	2.00001	-1.00001
9	0	2	0	$---$	2.00001	$---$
10	0	1.5	0	$---$	1.50001	$---$
11	0	1	0	$---$	1.00001	$---$
12	0	0.5	0	$---$	0.50008	$---$
13	0	0	0	$---$	$---$	$---$
14	0.5	0	0	0.50008	$---$	$---$
15	1	0	0	1.00001	$---$	$---$
16	1.5	0	0	1.50001	$---$	$---$

Table EI c. Example 1: displacements, analytical and SGBEM solution.

Reference[20]									
Node	**Analytical solution**			**SGBEM - 16 quadratic elements**			**SGBEM - 32 quadratic elements**		
	φ_x	φ_y	u_z	φ_x	φ_y	u_z	φ_x	φ_y	u_z
4	2.000	1.500	-3.000	2.010	1.492	-3.043	2.009	1.503	-3.022
5	2.000	2.000	-4.000	2.074	2.074	-4.056	2.047	2.047	-4.029
6	1.500	2.000	-3.000	1.492	2.010	-3.043	1.503	2.009	-3.022
7	1.000	2.000	-2.000	0.994	2.021	-2.034	0.993	2.006	-2.017
8	0.500	2.000	-1.000	0.469	2.015	-1.020	0.489	2.013	-1.010
9	0.000	2.000	0.000	0.000	2.103	0.000	0.000	2.063	0.000

Table EI d. Example 1: displacements, analytical and SGBEM solution in reference [20].

7.2 Example 2: square plate subjected to different loading conditions and compared with the Timoshenko's beam.

The "progenitor matrix" of the previous example allows performing with simple reorders and partitions, which depend on the boundary conditions, various examples whose results are compared with those obtained for the Timoshenko's beam. It is necessary to define a plate (Fig. 10a) whose sides b and d coincide with the ends 1 and 2 of the Timoshenko beam (Fig. 10b) having the same physical and geometric characteristics. In order to carry out the comparison it is necessary that on the sides a and c of the plate the boundary conditions will always be $\bar{M}_{nx} = \bar{M}_{ny} = \bar{T}_n = 0$ while on sides $\mathrm{d} \equiv 1$ and $\mathrm{b} \equiv 2$ the boundary conditions will vary according to the constraint. Equivalence entails $M_{nx} = M$, $T_n = T$.

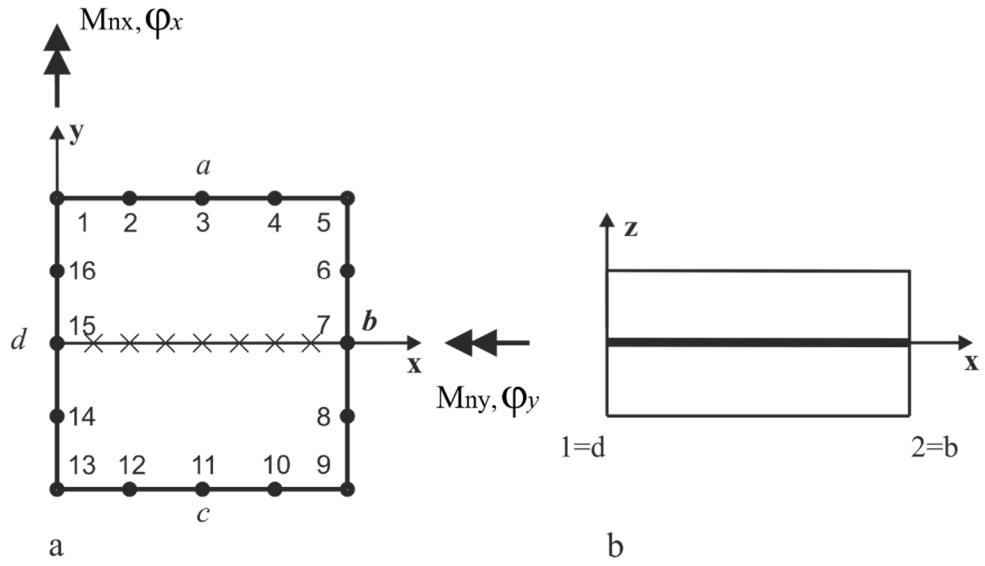

Fig. 10. a) Square plate of example 1 with 7 internal point where the response is evaluated, b) equivalent Timoskenko's beam of extremes 1,2.

The examples, from 2a to 2e, concern different load and constraint conditions. The analytical solution is a function of $f = EI$, $t = A/\chi$ of known meaning. The load vector is calculated considering the fundamental solutions modified provided in the Appendix 2 for $\bar{f}_z = \text{const}$, otherwise the RIM technique is applied to the case to be addressed.

Tables E IIa-e, as the plate is symmetric about the x axis, provides the results for nodes from 7 to 15 compared with the analytical solutions; diagrams are also provided. These provide the comparison between the analytical flexural curve and the values of $u_z(x)$ evaluated at 7 points inside the plate equally spaced along the axis $y = 0$ (Fig. 10a) through the S.I. of the vertical displacements.

7.2.1. Example 2a: Cantilever beam with linear distributed load $q = \bar{q}_0 \dfrac{x}{l}$.

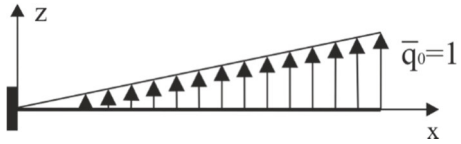

Fig. 11. Equivalent Timoskenko's beam: load conditions.

Timoshenko's beam solution:

$$u_z(x) = \left[\frac{(3l^2 - x^2)x}{2lt}\right]\bar{q}_0 + \left[\frac{(20l^3 - 10l^2x + x^3)x^2}{120lf}\right]\bar{q}_0; \qquad \varphi_x(x) = -\left[\frac{(8l^3 - 6l^2x + x^3)x}{24lf}\right]\bar{q}_0$$

$$T(x)=\frac{1}{2l}(l^2-x^2)\,\bar{q}_0;\qquad M(x)=-\frac{1}{6l}(l-x)^2(2l+x)\,\bar{q}_0. \tag{68a-d}$$

Node	Analytical solution				SGBEM – 8 quadratic elements			
	φ_x	u_z	M_{nx}	T_n	φ_x	u_z	M_{nx}	T_n
7	−1.00000	1.73333	− − −	− − −	−0.99985	1.73282	− − −	− − −
8	−1.00000	1.73333	− − −	− − −	−1.00116	1.73229	− − −	− − −
9	−1.00000	1.73333	− − −	− − −	−0.99928	1.73549	− − −	− − −
10	−0.98047	1.21289	− − −	− − −	−0.98011	1.21186	− − −	− − −
11	−0.85412	0.68750	− − −	− − −	−0.85379	0.68927	− − −	− − −
12	−0.54297	0.24389	− − −	− − −	−0.54098	0.24476	− − −	− − −
13	0.00000	0.00000	1.33333	−1.00000	− − −	− − −	1.33770	−1.00633
14	0.00000	0.00000	1.33333	−1.00000	− − −	− − −	1.33556	−1.00417
15	0.00000	0.00000	1.33333	−1.00000	− − −	− − −	1.33387	−0.99241

Table EII a. Example 2a: displacements, tractions, analytical and SGBEM solution.

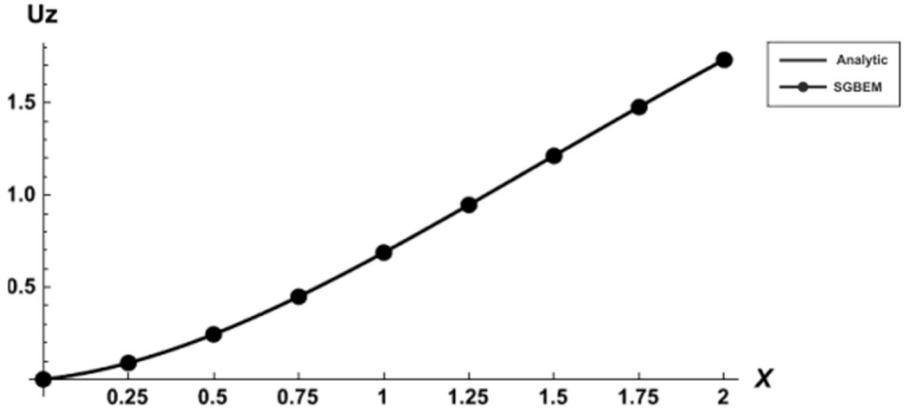

Fig. 12. Example 2a: analytical displacements $u_z(x)$ of Timoshenko's beam, displacements $u_z(x)$ along the line $y=0$ evaluated at 7 internal points by S.I.

7.2.2. Example 2b: Beam fixed at first extreme and simply supported at second extreme with uniformly distributed load $\bar{q}_0=1$.

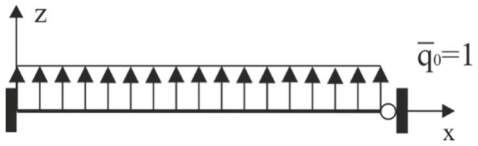

Fig. 13. Equivalent Timoskenko's beam: load conditions.

Timoshenko's beam solution:

$$u_z(x)=\left[\frac{(24f+10l^2t+ltx)(l-x)\,x}{16t(3f+l^2t)}\right]\bar{q}_0+\left[\frac{(3l^2-5lx+2x^2)}{48f}\right]\bar{q}_0;\qquad \varphi_x(x)=\left[\frac{3l(2l-x)\,x}{16(3f+l^2t)}\right]\bar{q}_0-\left[\frac{(6l^2-15lx+8x^2)x}{48f}\right]\bar{q}_0$$

$$T(x)=-\left[\frac{3fl}{8(3f+l^2t)}\right]\bar{q}_0+\left[\frac{5l-8x}{8}\right]\bar{q}_0;\qquad M(x)=-\left[\frac{3fl(l-x)}{8(3f+l^2t)}\right]\bar{q}_0-\left[\frac{l^2-5lx+4x^2}{8}\right]\bar{q}_0 \qquad (69a\text{-}d)$$

Node	Analytical solution				SGBEM – 8 quadratic elements			
	φ_x	u_z	M_{nx}	T_n	φ_x	u_z	M_{nx}	T_n
7	0.231884	0.00000	0.00000	−0.78261	0.23174	− − −	− − −	−0.77835
8	0.231884	0.00000	0.00000	−0.78261	0.22978	− − −	− − −	−0.78663
9	0.231884	0.00000	0.00000	−0.78261	0.23502	− − −	− − −	−0.77487
10	0.154891	0.15550	− − −	− − −	0.15429	0.15486	− − −	− − −
11	0.007246	0.19964	− − −	− − −	0.00754	0.20272	− − −	− − −
12	−0.08605	0.12833	− − −	− − −	−0.08494	0.12817	− − −	− − −
13	0.00000	0.00000	0.43478	−1.21739	− − −	− − −	0.43237	−1.22804
14	0.00000	0.00000	0.43478	−1.21739	− − −	− − −	0.43689	−1.21853
15	0.00000	0.00000	0.43478	−1.21739	− − −	− − −	0.43475	−1.21319

Table EII b Example 2b: displacements, tractions, analytical and SGBEM solution.

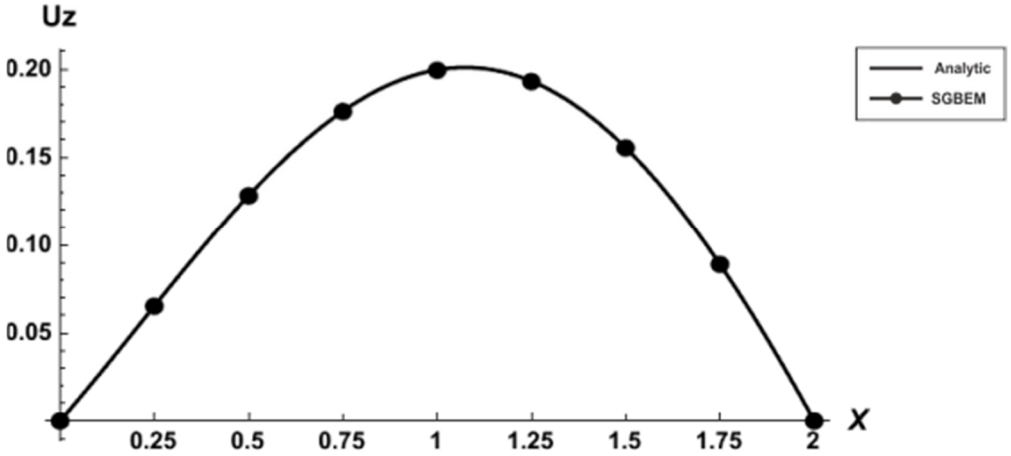

Fig. 14. Example 2c: analytical displacements $u_z(x)$ of Timoshenko's beam, displacement $u_z(x)$ along the line $y=0$ evaluated at 7 internal points by S.I.

7.2.3. Example 2c: Simply supported beam with parabolic load $q=\frac{4\bar{q}_0 x}{l}\left(1-\frac{x}{l}\right)$ and $\bar{q}_0=1$.

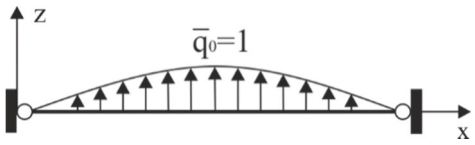

Fig. 15. Equivalent Timoskenko's beam: load conditions.

Timoshenko's beam solution:

$$u_z(x)=\left[\frac{(l-x)(l^2+lx-x^2)x}{3l^2t}\right]\bar{q}_0+\left[\frac{(l-x)(3l^4+3l^3x-2l^2x^2-2lx^3+x^4)x}{90fl^2}\right]\bar{q}_0;\qquad \varphi_x(x)=\left[\frac{(2x-l)(l^2+lx-x^2)^2}{30fl^2}\right]\bar{q}_0$$

$$T(x)=\frac{1}{3l^2}(l^3-6lx^2+4x^3)\bar{q}_0;\qquad M(x)=\frac{1}{3l^2}(l^3-2lx^2+x^3)\bar{q}_0 \tag{70a-d}$$

Node	Analytical solution				SGBEM – 8 quadratic elements			
	φ_x	u_z	M_{nx}	T_n	φ_x	u_z	M_{nx}	T_n
7	0.26666	0.00000	0.00000	−0.66666	0.26608	− − −	− − −	−0.65969
8	0.26666	0.00000	0.00000	−0.66666	0.26492	− − −	− − −	−0.67139
9	0.26666	0.00000	0.00000	−0.66666	0.26888	− − −	− − −	−0.65818
10	0.18802	0.17929	− − −	− − −	0.18687	0.17950	− − −	− − −
11	0.00000	0.25273	− − −	− − −	0.00000	0.25749	− − −	− − −
12	−0.18802	0.17929	− − −	− − −	−0.18687	0.17950	− − −	− − −
13	−0.26666	0.00000	0.00000	−0.66666	−0.26888	− − −	− − −	−0.65818
14	−0.26666	0.00000	0.00000	−0.66666	−0.26492	− − −	− − −	−0.67139
15	−0.26666	0.00000	0.00000	−0.66666	−0.26608	− − −	− − −	−0.65969

Table EII c. Example 2d: displacements, tractions, analytical and SGBEM solution.

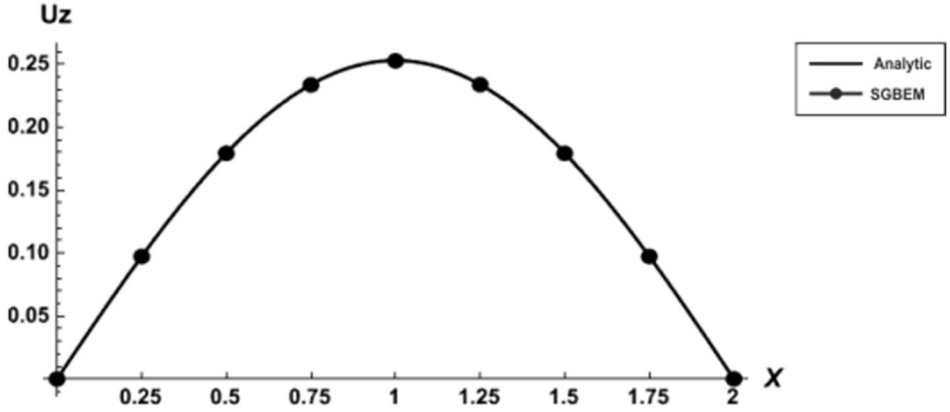

Fig. 16. Example 2c: analytical displacements $u_z(x)$ of Timoshenko's beam, displacements $u_z(x)$ along the line $y=0$ evaluated at 7 internal points by S.I.

7.2.4. Example 2d: Simply supported beam with sinusoidal load $q=\bar{q}_0\,sin\left(2\pi\frac{x}{l}\right)$ and $\bar{q}_0=1$.

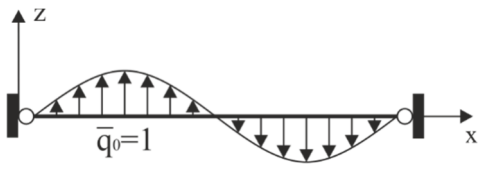

Fig. 17. Equivalent Timoskenko's beam: load conditions.

Timoshenko's beam solution:

$$u_z(x)=\frac{l^2}{4\pi t}sin\left(2\pi\frac{x}{l}\right)+\frac{l^4}{16\pi^4 f}sin\left(2\pi\frac{x}{l}\right);\qquad \varphi_x(x)=-\frac{l^3}{8\pi^3 f}cos\left(2\pi\frac{x}{l}\right)$$

(71 a-d)

$$T(x)=\frac{l}{2\pi}cos\left(2\pi\frac{x}{l}\right);\qquad M(x)=\frac{l^2}{4\pi^2}sin\left(2\pi\frac{x}{l}\right) \tag{71a-d}$$

Node	Analytical solution				SGBEM – 8 quadratic elements			
	φ_x	u_z	M_{nx}	T_n	φ_x	u_z	M_{nx}	T_n
7	−0.03225	0.00000	0.00000	0.31831	−0.03358	− − −	− − −	0.31764
8	−0.03225	0.00000	0.00000	0.31831	−0.03241	− − − −	− − −	0.31884
9	−0.03225	0.00000	0.00000	0.31831	−0.03522	− − − −	− − −	0.32282
10	0.00000	−0.03053	− − −	− − −	−0.00067	−0.02944	− − −	− − −
11	0.03225	0.00000	− − −	− − −	0.03891	0.0000	− − −	− − −
12	0.00000	0.03053	− − −	− − −	−0.0067	0.02944	− − −	− − −
13	−0.03225	0.00000	0.00000	−0.31831	−0.03522	− − −	− − −	−0.32282
14	−0.03225	0.00000	0.00000	−0.31831	−0.03241	− − −	− − −	−0.31884
15	−0.03225	0.00000	0.00000	−0.31831	−0.03358	− − −	− − −	−0.31764

Table EII d. Example 2d: displacements, tractions, analytical and SGBEM solution.

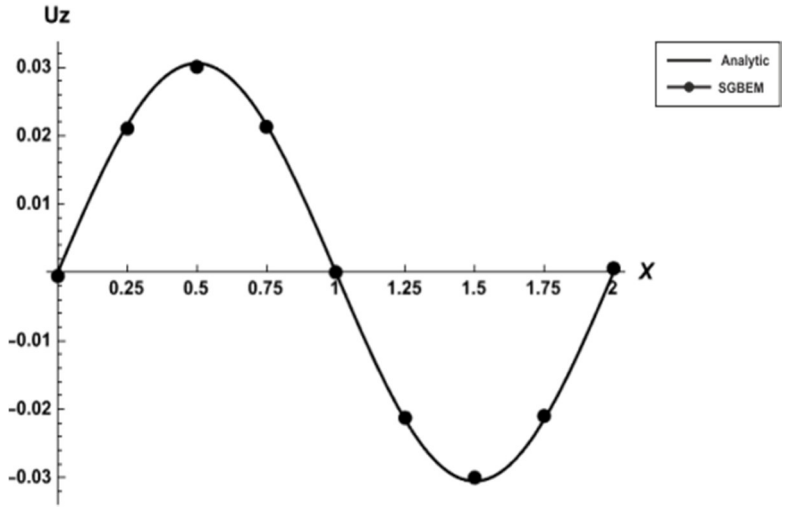

Fig. 18. Example 2d: analytical displacements $u_z(x)$ of Timoshenko's beam, displacement $u_z(x)$ along the line $y=0$ evaluated at 7 internal points by S.I.

7.3. Example 3: Clamped circular plate with uniformly distributed load $q=1$.

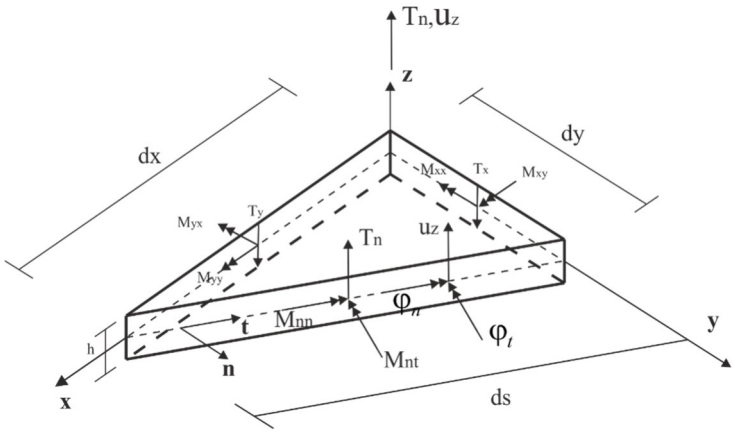

Fig. 19. Local reference system $\{\mathbf{n},\mathbf{t}\}$: vectors $\mathbf{m}$, $\mathbf{t}_n$, $\mathbf{u}_n$.

The plate is referred to the local reference system $\{\mathbf{n},\mathbf{t}\}$ of Fig. 19 with respect to which is written

$$\mathbf{m}=\begin{bmatrix} M_{nn} \\ M_{nt} \end{bmatrix}=\begin{bmatrix} n_x & n_y \\ t_x & t_y \end{bmatrix}\cdot\begin{bmatrix} M_{nx} \\ M_{ny} \end{bmatrix}=\mathbf{G}\,\mathbf{m}_n\,,\ \mathbf{u}_n=\begin{bmatrix} \varphi_n \\ \varphi_n \\ u_z \end{bmatrix}=\begin{bmatrix} n_x & n_y & 0 \\ t_x & t_y & 0 \\ 0 & 0 & 1 \end{bmatrix}\cdot\begin{bmatrix} \varphi_x \\ \varphi_y \\ u_z \end{bmatrix}=\mathbf{H}\cdot\mathbf{u} \qquad (72a, b)$$

and $\mathbf{t}_n$ unchanged.

The data of the circular plate of Fig. 20, discretized by 16 quadratic boundary elements are: radius $a=1$, height $h=1$, shear factor $\lambda=\sqrt{10}$, Young's modulus $E=12$, Poisson's ratio $n=0.3$. The following kinematic conditions are valid on the boundary: $\bar{\varphi}_n=0,\ \bar{\varphi}_t=0,\ \bar{u}_z=0$.

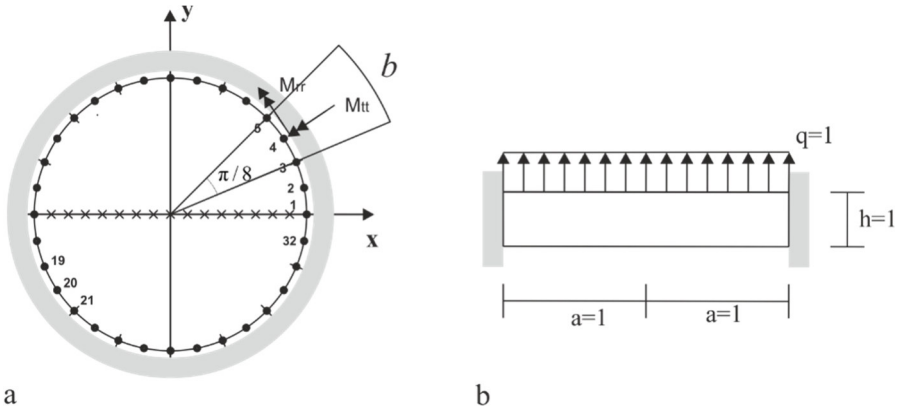

Fig. 20. Clamped circular plate with uniformly distributed load: a) discretization with 16 quadratic boundary elemnts, generic boundary element *b* and 17 internal point where the response is evaluated, b) cross section.

The assumption of the reference system of Fig. 19 entails radial bending moments $M_{rr}=M_{nn}$ and diametral torsional moments $M_{\theta\theta}=M_{tt}$. For this problem the analytical solution is [10]:

$$u_z=\frac{q\,a^2}{64\,A}\left[1-\left(\frac{r}{a}\right)^2\right]\cdot\left[1+2\,C-\left(\frac{r}{a}\right)^2\right];\qquad \varphi_r=\frac{q\,a^3}{16\,A}\left[1-\left(\frac{r}{a}\right)^2\right]\cdot\left(\frac{r}{a}\right)$$

$$M_{rr}=M_{nn}=\frac{q\,a^2}{16}\left[(1+n)-(3+n)\left(\frac{r}{a}\right)^2\right];\quad M_{\theta\theta}=M_{tt}=\frac{q\,a^2}{16}\left[(1+n)-(1+3n)\left(\frac{r}{a}\right)^2\right];\quad Q_n=T_n=-\frac{q\,a}{2}\left(\frac{r}{a}\right) \qquad (73a\text{-}e)$$

where

$$\mathrm{C}=\frac{1.6}{1-n}\left(\frac{h}{a}\right) \qquad (74)$$

Computational reasons lead to the calculation of the entire plate even if symmetries exist; consequently, the diametral moments $M_{\theta\theta}=M_{tt}$ are zero both on the boundary and inside the plate. After calculating the "progenitor matrix", for this constraint condition on the boundary it results $\mathbf{K}=\mathbf{B}_{uu}$; the domain load vector $\mathbf{L}_\Omega$ for $q=1$ it calculated using the RIM technique. Tractions or displacements imposed on the contour could also be considered, but the relative analytical solutions for making a comparison do not exist.

In the following table, the analytic solution is compared with the obtained results; as the results are identical on the whole boundary, these are only provided for boundary element *b* (Fig. 20).

Node	Analytical solution		SGBEM 16 quadratic elements	
	M_{nn}	T_n	M_{nn}	T_n
3	−0.125	−0.500	−0.125005	−0.500019
4	−0.125	−0.500	−0.124998	−0.499991
5	−0.125	−0.500	−0.125005	−0.500019

Table EIII. Example 3: tractions, analytical and SGBEM solution.

Now let's calculate the vertical balance of the plate:

- resulting applied load on the domain R_a

$$R_a = A \cdot \overline{f}_z = \pi a^2 \overline{f}_z = \pi = 3.14159 \tag{75}$$

- resulting tractions on the boundary R_c

$$R_c = 16\left[\int_{\frac{\pi}{8}}^{\frac{2\pi}{8}} T_{n3}\Psi_{b3}\, d\varphi + \int_{\frac{\pi}{8}}^{\frac{2\pi}{8}} T_{n4}\Psi_{b4}\, d\varphi + \int_{\frac{\pi}{8}}^{\frac{2\pi}{8}} T_{n5}\Psi_{b5}\, d\varphi\right] = 3.14159 \tag{76}$$

In the Eq. (76) T_{ni} and Ψ_{bi} , $i = 3,4,5$ are the reactive tractions and shape functions associated with the nodes i related to the boundary element b ; for obtain the total reactive traction it is necessary to consider the total 16 boundary elements. It results to be $R_a = R_c$ and therefore the system is balanced. It is useful to compare this result with the one in [10] where vertical equilibrium is not achieved.

The diagrams of Fig. 21-23 provide the comparison between the analytical solutions (Eqs. (73a-e)) and the results obtained through the S.I. at 15 point along the x axis (Fig. 20a)

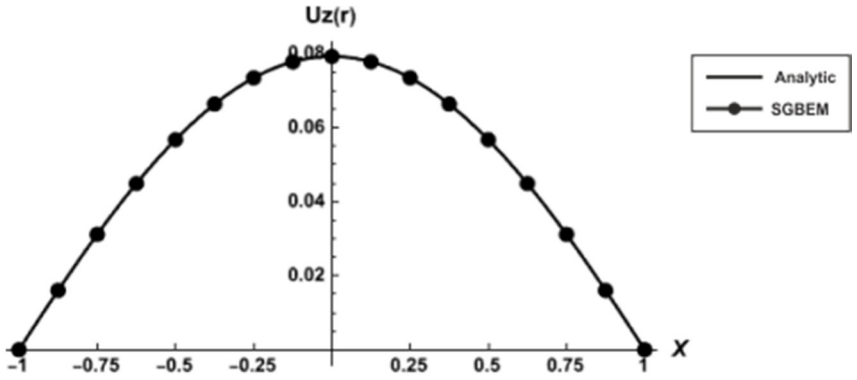

Fig. 21. Example 3: analytical solution $u_z(x)$, displacements $u_z(x)$ along the line $y = 0$ evaluated at 15 points by S. I

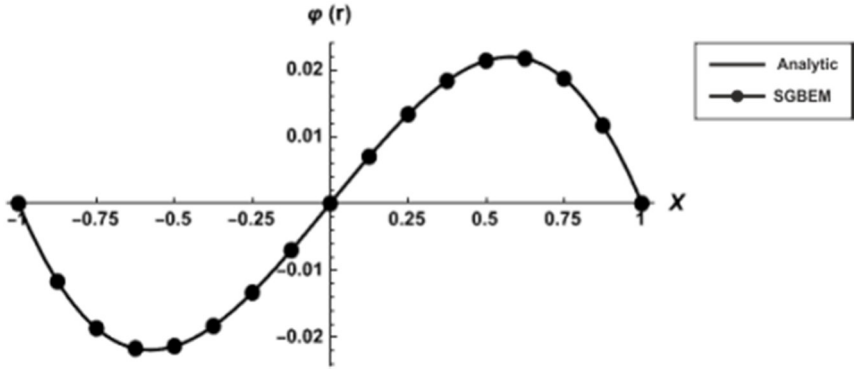

Fig. 22. Example 3: analytical solution $\varphi_r(x)$, rotations $\varphi_r(x)$ along the line $y = 0$ evaluated at 15 points by S. I.

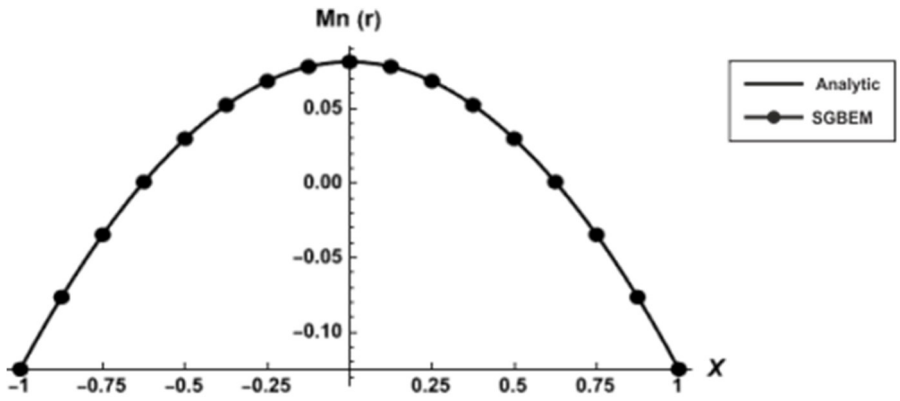

Fig. 23. Example 3: analytical solution $M_n(x)$, circumferential bending moment $M_n(x)$ along the line $y = 0$ evaluated at 15 points by S. I.

8. Conclusions.

The SGBEM is applied to shear deformable plates. The "progenitor matrix" approach considers the total range of boundary conditions of structures having certain physical and geometric characteristics; its coefficients are calculated without using regularization techniques and referring to the theory of distributions. Various distribution laws of the vertical load on the domain are considered and the integrals has been transformed into a boundary integrals through the RIM technique. The use of the "progenitor matrix" and the RIM technique allows obtaining a robust resolving system that does not present problems of numerical instability and obtains excellent results in the analysis even in the presence of a sparse discretization as demonstrated by the examples.

Appendix 1: Power series expansion of Bessel functions in $\mathbb{R}$.

The fundamental solutions of the Mindlin-Reissner plate BEM present the functions $K_n(z)$ denoting the modified Bessel functions of the second kind and order $n-th$. These functions, defined for $n \in \mathbb{R}$, exhibit asymptotic behaviour, i.e.:

$$\lim_{z\to\infty} K_n(z) = 0; \qquad \lim_{z\to 0} K_n(z) = +\infty \tag{A1.1, 2}$$

in addition, manifest singularities from the weakest up $ln(z)$ to the highest order hypersingularity z^{-n}.

The presence of logarithmic terms confines the graphs of these functions to the positive real Cartesian half-plane. For a complete discussion of these functions (Magno [30]).

For the purposes of this publication, in order to carry out the necessary simplifications of the fundamental solutions, the recursive identity has been used, i.e.

$$K_{n+1}(z) = \frac{2n}{z} K_n(z) + K_{n-1}(z) \tag{A1.3}$$

The series expansion of the Bessel functions allows calculating the coefficients of the solving system; this expansion depends on the order n of the functions through the following formulas:

- if $n = 0$:

$$K_0(z) = \underbrace{-ln\left(\frac{z}{2}\right)}_{\text{singular}} - \gamma - \sum_{k=1}^{q=+\infty} \frac{1}{(2^k k!)^2}\left(ln\left(\frac{z}{2}\right) + \gamma - \sum_{p=1}^{k}\left(\frac{1}{p}\right)\right) z^{2k} \tag{A1.4}$$

- if $n = 1, 2, 3, ...$:

$$K_n(z) = (-1)^{n+1}\left(\begin{array}{l} \dfrac{1}{n!}\left(ln\left(\dfrac{z}{2}\right) + \gamma - \dfrac{1}{2}\sum_{p=1}^{n}\left(\dfrac{1}{p}\right)\right)\left(\dfrac{z}{2}\right)^n + \\ + \sum_{k=1}^{q=+\infty} \dfrac{1}{2^{2k+n} + k!(k+n)!}\left(ln\left(\dfrac{z}{2}\right) + \gamma - \sum_{p=1}^{k}\left(\dfrac{1}{p}\right) - \dfrac{1}{2}\sum_{p=1}^{n}\left(\dfrac{1}{k+p}\right)\right) z^{2k+n} \end{array}\right) + \underbrace{\frac{1}{2}\sum_{p=0}^{n-1} \frac{(-1)^p (n-p-1)!}{2^{2p-n}\, p!} z^{2p-n}}_{\text{singular and regular terms}} \tag{A1.5}$$

where γ is the Euler constant and $z = \lambda \mathbf{r}$.

From the expressions (A1.4, 5) it turns out that, $K_0(z)$ exhibits logarithmic singularities $ln(z), K_n(z)$ exhibits a highlighted term that generates singular terms starting from the highest order αz^{-n} and regular terms. In the highlighted term of the expression (A1. 5), the summation counter p depends only on the order n of the Bessel function and therefore the terms generated are limited when compared to the others in the series expansion. The highest order of singularity is obtained setting

$$\alpha = \frac{(n-1)!}{2^{(1-n)}} \tag{A1.6}$$

The summation counter $k = \subseteq \{0, q = +\infty\}$ for $q = +\infty$ gives the exact approximation of the Bessel function.

The distinction of singular S and regular R contributions in Bessel functions, with obvious meaning of symbols leads to writing:

$$K_0(z) = K_0^R(z) + K_0^S(z); \qquad K_n(z) = K_n^R(z) + K_n^S(z) \tag{A1.7, 8}$$

Appendix 2: Fundamental solutions.

The fundamental solutions are functions of $\mathbf{z} = \lambda\,\mathbf{r}$ where $\mathbf{r} = \sqrt{\mathbf{x}^2 - \boldsymbol{\xi}^2}$ is the distance vector between effect point $\mathbf{x} = (x, y)$ and source point $\boldsymbol{\xi} = (\xi, \eta)$, $\lambda = \sqrt{10}/h$ shear factor, h height of the plate.

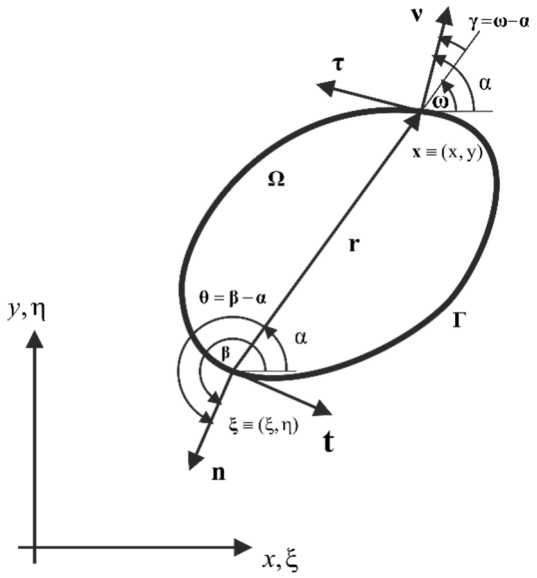

Fig. 24: Geometric definitions between the positions of the source point $\boldsymbol{\xi} \equiv (\xi, \eta)$ and effect $\mathbf{x} \equiv (x, y)$ both placed on the boundary Γ

In Fig. 24 vectors $\mathbf{n}, \mathbf{t}, \boldsymbol{\nu}, \boldsymbol{\tau}$ represent the normal vector and the tangent vector to the boundary at the respective points and derivatives are taken with respect to the same points:

$$r_i = x_i - \xi_i, \qquad r = (r_i\, r_i)^{1/2}$$

$$r_{,x} = \frac{\partial r}{\partial x} = \frac{r_x}{r} = -r_{,\xi}, \qquad r_{,y} = \frac{\partial r}{\partial y} = \frac{r_y}{r} = -r_{,\eta} \tag{A2.1-8}$$

$$\frac{\partial r}{\partial \nu} = r_{,\nu}, \qquad \frac{\partial r}{\partial \tau} = r_{,\tau}, \qquad \frac{\partial r}{\partial n} = r_{,n}, \qquad \frac{\partial r}{\partial t} = r_{,t}$$

First, the fundamental solution $\mathbf{G}_{uu}(\mathbf{x};\boldsymbol{\xi})$ for the generation of the "progenitor matrix" is provided, and then the fundamental solutions modified through the R.I.M technique that allow obtaining the domain loads vector by replacing the domain integral with a boundary one in the case of $\overline{f}_z = \text{const}$.

A2.1 Fundamental solutions $\mathbf{G}_{uu}(\mathbf{x};\boldsymbol{\xi})$ for the generation of the "progenitor matrix".

$$\mathbf{G}_{uu}(\mathbf{x};\boldsymbol{\xi}) = \begin{bmatrix} G_{uu}^{1,1} & G_{uu}^{1,2} & G_{uu}^{1,3} \\ G_{uu}^{2,1} & G_{uu}^{2,2} & G_{uu}^{2,3} \\ G_{uu}^{3,1} & G_{uu}^{3,2} & G_{uu}^{3,3} \end{bmatrix} \tag{A2.9}$$

$$G_{uu}^{1,1}(\mathbf{x};\boldsymbol{\xi}) = \frac{1}{8A(1-n)\pi}\{4K_0(z) - 4(1-2r_{,x}^2)K_{2q}(z) + (1-n)((1-2r_{,x}^2) + ln(z^2))\} \tag{A2.10-18}$$

$$G_{uu}^{1,2}(\mathbf{x};\boldsymbol{\xi}) = \frac{r_{,x} r_{,y}}{4A(1-n)\pi}\{4K_{2q}(z) - (1-n)\}$$

$$G_{uu}^{1,3}(\mathbf{x};\boldsymbol{\xi}) = \frac{r\, r_{,x}}{8\pi A}(1 - ln(z^2))$$

$$G_{uu}^{2,1}(\mathbf{x};\boldsymbol{\xi}) = G_{uu}^{1,2}(\boldsymbol{\xi};\mathbf{x})$$

$$G_{uu}^{2,2}(\mathbf{x};\boldsymbol{\xi}) = \frac{1}{8A(1-n)\pi}\{4K_0(z) - 4(1-2r_{,y}^2)K_{2q}(z) + (1-n)((1-2r_{,y}^2) - ln(z^2))\}$$

$$G_{uu}^{2,3}(\mathbf{x};\boldsymbol{\xi}) = \frac{r\, r_{,y}}{8\pi A}(1 - log(z^2))$$

$$G_{uu}^{3,1}(\mathbf{x};\boldsymbol{\xi}) = G_{uu}^{1,3}(\boldsymbol{\xi};\mathbf{x})$$

$$G_{uu}^{3,2}(\mathbf{x};\boldsymbol{\xi}) = G_{uu}^{2,3}(\boldsymbol{\xi};\mathbf{x})$$

$$G_{uu}^{3,3}(\mathbf{x};\boldsymbol{\xi}) = \frac{1}{8A(1-n)\pi\lambda^2}\{(1-n)z^2(log(z) - 1) - 8\, ln(z)\}$$

where (A1.4, 5) $K_0(z)$ has a singularity of type $ln(z)$ and $K_{2q}(z) = \frac{2}{z^2} - K_2(z)$ is regular since

$$\lim_{z\to 0} K_{2q}(z) = \frac{1}{2} \tag{A2.19}$$

The fundamental solutions $\mathbf{G}_{uu}(\mathbf{x},\boldsymbol{\xi})$ allows finding the complete matrix of fundamental solutions $\mathbf{G}(\mathbf{x},\boldsymbol{\xi})$ (Table 1) through the procedure adopted in [2] and therefore the fundamental solutions for the generation of "progenitor matrix".
As an example the fundamental solution $G_{tt}^{1,1}(\mathbf{x};\boldsymbol{\xi},\mathbf{n})$, that provides the traction M_{nx} on an element with normal vector $\boldsymbol{\nu}$ placed at the effect point $\mathbf{x} = (x, y)$ caused by double-layered rotations $\mathrm{v} = -\varphi_x$ which acts on an element with normal vector $\mathbf{n}$ placed at the source point $\boldsymbol{\xi} = (\xi, \eta)$, is derived.
After a series of simplifications, involving the application of the recursive identity of Bessel function (A1. 3) and of the technique adopted by Katsikadelis [31] that exploits the existing trigonometric relationships between derivatives, easily deducible from Fig. 24, the fundamental solution is expressed in a compact form using only the derivatives

$$\begin{aligned} G_{tt}^{1,1}(\mathbf{x};\boldsymbol{\xi},\mathbf{n}) = \frac{A(1-n)\lambda^2}{8\pi}\{&(\frac{48}{z^4} - K_4(z))((r_{,x}^2 - r_{,y}^2)(r_{,n}r_{,\nu} - r_{,t}r_{,\tau}) - 2r_{,x}r_{,y}(r_{,t}r_{,\nu} - r_{,n}r_{,\tau})) + K_0(z)(r_{,n}r_{,\nu} + r_{,t}r_{,\tau}) + \\ &+ \frac{2(1-n)}{z^2}(r_{,t}r_{,\tau} - r_{,n}r_{,\nu} - 2((r_{,x}^2 - r_{,y}^2)r_{,n}r_{,\nu} - r_{,x}r_{,y}(r_{,t}r_{,\nu} + r_{,n}r_{,\tau}))) + \frac{8}{z^2}(r_{,x}^2 r_{,n}r_{,\nu} - r_{,y}^2 r_{,t}r_{,\tau})\} \end{aligned} \tag{A2.20}$$

where

$$K_{4q} = \frac{48}{z^4} - K_4(z) \tag{A2.21}$$

Taking into account Eq. (A1.5), and in particular, the last part that generates singular and regular terms, it results:

$$K_{4q} = \frac{48}{z^4} - K_4(z) = K_{4q}^R + K_{4q}^S = K_{4q}^R + \frac{1}{4} + \frac{48}{z^2} - \frac{z^2}{48} \tag{A2.22}$$

where the apex R an S identify the singular and regular parts. In the Eq. (A2.22), the singularity αz^{-4} is removed and a singularity αz^{-2} remains.
These operations make it possible to distinguish between a regular part and a singular part in the fundamental solution, i.e.:

$$G_{tt}^{1,1}(\mathbf{x};\boldsymbol{\xi},\mathbf{n}) = G_{tt}^{1,1-R}(\mathbf{x};\boldsymbol{\xi},\mathbf{n}) + G_{tt}^{1,1-S}(\mathbf{x};\boldsymbol{\xi},\mathbf{n}) \tag{A2.23}$$

A2.2 Fundamental solutions which allow obtaining the domain load vector replacing the domain integral with a boundary one in the case of $\overline{f}_z = const$.

In the expressions that follow, the superscript $-B$ indicates that that the given fundamental solution is suitable for boundary integration.

Matrix $\mathbf{G}_{uu}^{\alpha,3-B}(\mathbf{x};\boldsymbol{\xi},\mathbf{n})$ with $\alpha = 1,2,3$

$$G_{uu}^{1,3-B}(\mathbf{x};\boldsymbol{\xi},\mathbf{n}) = \frac{r_{,x}(5-6ln(z))}{72A\pi} r\, r_{,n} \tag{A2.24-26}$$

$$G_{uu}^{2,3-B}(\mathbf{x};\boldsymbol{\xi},\mathbf{n}) = \frac{r_{,y}(5-6ln(z))}{72A\pi} r\, r_{,n}$$

$$G_{uu}^{3,3-B}(\mathbf{x};\boldsymbol{\xi},\mathbf{n}) = \left(\frac{1-ln(z^2)}{4A(1-\nu)\pi\lambda^2} - \frac{r^2(5-6ln(z^4))}{128A\pi} \right) r\, r_{,n}$$

Matrix $\hat{\mathbf{G}}_{uu}^{\alpha,1-B}(\mathbf{x};\boldsymbol{\xi},\mathbf{n})$ with $\alpha = 1,2,3$

$$\hat{G}_{uu}^{1,1-B}(\mathbf{x};\boldsymbol{\xi},\mathbf{n}) = \frac{r_{,x}}{2\pi A} r_{,n} \tag{A2.27-29}$$

$$\hat{G}_{uu}^{2,1-B}(\mathbf{x};\boldsymbol{\xi},\mathbf{n}) = \frac{r_{,y}}{2\pi A} r_{,n}$$

$$\hat{G}_{uu}^{3,1-B}(\mathbf{x};\boldsymbol{\xi},\mathbf{n}) = \frac{(1-ln(z^2))}{8\pi A} r\, r_{,n}$$

Matrix $\mathbf{G}_{tu}^{\alpha,3-B}(\mathbf{x},\mathbf{v};\boldsymbol{\xi},\mathbf{n})$ with $\alpha = 1,2,3$

$$G_{tu}^{1,3-B}(\mathbf{x},\mathbf{v};\boldsymbol{\xi},\mathbf{n}) = \frac{1}{16\pi}\Big(-(1-\nu)(r_{,x}r_{,\nu} - r_{,y}r_{,\tau}) + (1+\nu)(r_{,x}r_{,\nu} + r_{,y}r_{,\tau})(1-ln(z^2))\Big) r\, r_{,n} \tag{A2.30-32}$$

$$G_{tu}^{2,3-B}(\mathbf{x},\mathbf{v};\boldsymbol{\xi},\mathbf{n}) = \frac{1}{16\pi}\Big(-(1-\nu)(r_{,y}r_{,\nu} + r_{,x}r_{,\tau}) + (1+\nu)(r_{,y}r_{,\nu} - r_{,x}r_{,\tau})(1-ln(z^2))\Big) r\, r_{,n}$$

$$G_{tu}^{3,3-B}(\mathbf{x},\mathbf{v};\boldsymbol{\xi},\mathbf{n}) = -\frac{r_{,\nu}}{2\pi} r_{,n}$$

Matrix $\hat{\mathbf{G}}_{tu}^{\alpha,1-B}(\mathbf{x},\mathbf{v};\boldsymbol{\xi},\mathbf{n})$ with $\alpha = 1,2,3$

$$\hat{G}_{tu}^{1,1-B}(\mathbf{x},\mathbf{v};\boldsymbol{\xi},\mathbf{n}) = -\frac{(1-\nu)}{2\pi r}\Big((r_{,x}r_{,\nu} - r_{,y}r_{,\tau})ln(r)\Big) r_{,n} \tag{A2.33-35}$$

$$\hat{G}_{tu}^{2,1-B}(\mathbf{x},\mathbf{v};\boldsymbol{\xi},\mathbf{n}) = -\frac{(1-\nu)}{2\pi r}\Big((r_{,y}r_{,\nu} + r_{,x}r_{,\tau})ln(r)\Big) r_{,n}$$

$$\hat{G}_{tu}^{3,1-B}(\mathbf{x},\mathbf{v};\boldsymbol{\xi},\mathbf{n}) = 0$$

References

[1] Sirtori S. General Stress analysis method by means of integral equations and boundary elements. Meccanica 1979; 14: 210-218. https://doi.org/10.1007/BF02128438

[2] Polizzotto C. An energy approach to the boundary element method, Part. I: Elastic solids. Comput Methods Appl Mech Eng 1988; 69:167-184. https://doi.org/10.1016/0045-7825(88)90186-7

[3] Bonnet M, Maier G, Polizzotto C. Symmetric Galerkin boundary element method. Appl Mech Rev 1998; 51: 669-704. https://doi.org/10.1016/0045-7825(88)90186-7

[4] Terravecchia S S. Closed form coefficient in the symmetric boundary element approach. Eng Analysis Boundary Elem 2006; 30: 479-488. https://doi.org/10.1016/j.enganabound.2006.01.002

[5] Panzeca T, Cucco F, Terravecchia S S, Symmetric boundary element method versus finite element method. Comput Methods Appl Mech Eng 2002; 191: 3347-3367. https://doi.org/10.1016/S0045-7825(02)00239-6

[6] Panzeca T, Terravecchia S S, Zito L. Computational aspects in 2D SBEM analysis with domain inelastic action. Int J Numer Methods Eng 2010; 82: 184-204. https://doi.org/10.1002/nme.2765
[7] Reissner E. The effect of transverse shear deformation on the bending of elastic plates. J Appl Mech 1945; 12: A69-A76. https://doi.org/10.1115/1.4009435
[8] Reissner E. On transverse bending of plates, including the effect of transverse shear deformation. Int J Solids Struct 1975; 11: 569-573. https://doi.org/10.1016/0020-7683(75)90030-X
[9] Mindlin R D. Influence of rotatory inertia and shear on flexural motion of isotropic elastic plates. J Appl Mech 1951; 18: 31-38. https://doi.org/10.1115/1.4010217
[10] Vander Weeën F. Application of the boundary integral equation method to Reissner's plate model. Int J Numer Methods Eng 1982; 18: 1-10. https://doi.org/10.1002/nme.1620180102
[11] Hörmander H. *Linear Partial Differential Operators*. Springer-Verlag: Berlin; 1963.
[12] El Zafrany A, Debbih M, Fadhil S. Application of the boundary integral equation method to Reissner's plate model. Int J Numer Methods Eng 1994; 18:1-10. https://doi.org/10.1002/nme.1620180102
[13] El Zafrany A, Debbih M, Fadhil S. An efficient approach for boundary element bending analysis of thin and tick plates. Comput Stuct 1994; 56: 565-576-10. https://doi.org/10.1016/0045-7949(94)00559-L
[14] Westphal Jr T, Andra H, Scnack E. Some fundamental solutions for the Kirchhoff, Reissner and Mindlin plates and a unified BEM formulation, Eng Analysis Boundary Elem 2001; 25: 129-139.
[15] Long S Y, Brebbia C A, Telles J C F. Boundary element bending analysis of moderately thick plates. Eng Anal 1988; 5: 64-74. https://doi.org/10.1016/0264-682X(88)90040-8
[16] Rashed Y F, Aliabadi M H, Brebbia C A. Hypersingular boundary element method formulation for Reissner plate. Int J Solids Struct 1998; 18: 2229-2249. https://doi.org/10.1016/S0020-7683(97)00188-1
[17] Aliabadi M H, All W S, Phemister T H. Taylor expansion for singular kernels in the boundary element method. Int J Numer Methods Eng 1985; 21: 2221-2236. https://doi.org/10.1002/nme.1620211208
[18] Aliabadi M H. Plate bending analysis with boundary elements. Advances in Boundary Elements. Computational Mechanics Publications: Southampton, UK; 1998.
[19] Aliabadi M H. The Boundary Element Method, Volume 2: Applications in Solids and Structures. John Wiley and Sons: Chichester, UK; 2002.
[20] Perez-Gavilan J J, Aliabadi M H. Symmetric Galerkin BEM for shear deformable plates. Int J Numer Methods Eng 2003; 57:1661-1693. https://doi.org/10.1002/nme.734
[21] Perez-Gavilan J J, Aliabadi M H. A Galerkin formulation for shear deformable plate bending dynamics. Int J Numer Methods Eng 2004; 61: 1093-1106. https://doi.org/10.1002/nme.1109
[22] Panzeca T, Salerno M, Terravecchia S. Symmetric Galerkin Boundary -Element Method for 3-D analysis. Boundary Element Techniques 1999; 477-486. ISBN: 0-904-188-531
[23] Brebbia C A, Telles J F C, Wrobel L C. (1984), Boundary Element Tecniques, Springer-Verlag: Berlin Heidelberg, DE; 1984.
[24] Gao X W, Davies T G. An effective boundary element algoritm for 2D and 3D elastoplastic problems, Int J Solids Struct 2000; 37: 4987-5008. https://doi.org/10.1016/S0020-7683(99)00188-2
[25] Wen P H, Aliabadi M H, Young A. Transformation of domain integrals to boundary integrals in BEM analysis of shear deformable plate bending problem. Comp Mech 1999; 24: 304-309. https://doi.org/10.10077s004660050519
[26] Cucco F, Panzeca T, Terravecchia S S. Program Karnak SGBEM. Palermo, 2002.
[27] Terravecchia S. Analisi per sottostrutture nel Metodo Simmetrico degli elementi di Contorno-Lastre, PhD Thesis, Cosenza; 2014.
[28] Panzeca T, Cucco F, Terravecchia S S. Boundary discretization based on the energetic residuals using the SGBEM. Int J Solids 2007; 44: 7239-7260. https://doi.org/10.1016/j.ijsolstr.2007.04.003
[29] Panzeca T, Cucco F, Terravecchia S S. Strain energy evaluation in structures having zone-wise variable physically-mechanical quantities. Advances in Boundary Element Techniques & Meshless Techniques XIV 2013. 62-69. ISBN: 978-0-9576731-0-6
[30] Magno C. (2020), Rappresentazioni in serie di potenze delle funzioni di Bessel in $\mathbb{R}$. www.cm-physmath.net. 2020.
[31] Katsikadelis J T. (2014), The Boundary Element Method for Plate Analysis, Elsevier Publications: Oxford, UK; 2014.